

# Capacity Gains in MIMO Systems with Few-Bit ADCs Using Nonlinear Analog Circuits

Marian Temprana Alonso\*, Xuyang Liu<sup>†</sup>, Hamidreza Aghasi<sup>†</sup>, Farhad Shirani\* \*School of Computing and Information Sciences, Florida International University, Miami, FL, {mtempran,fshirani}@fiu.edu

<sup>†</sup>Department of Electrical Engineering and Computer Science, University of California, Irvine, {xuyanl3,haghasi}@uci.edu

**Abstract**—Analog to Digital Converters (ADCs) are a major contributor to the power consumption of multiple-input multiple-output (MIMO) receivers with large antenna arrays operating in the millimeter wave carrier frequencies. This is especially the case in large bandwidth communication systems, due to the sudden drop in energy-efficiency of ADCs as the sampling rate is increased above 100MHz. Two mitigating energy-efficient approaches which have received significant recent interest are i) to reduce the number of ADCs via analog and hybrid beamforming architectures, and ii) to reduce the resolution of the ADCs which in turn decreases power consumption. However, decreasing the number and resolution of ADCs leads to performance loss — in terms of achievable rates — due to increased quantization error. In this work, we study the application of practically implementable nonlinear analog operators such as envelope detectors and polynomial operators, prior to sampling and quantization at the ADCs, as a way to mitigate the aforementioned rate-loss. A receiver architecture consisting of linear analog combiners, nonlinear analog operators, and few-bit ADCs is designed. The fundamental information theoretic performance limits of the resulting communication system, in terms of achievable rates, are investigated under various assumptions on the set of implementable analog operators. Extensive numerical evaluations and simulations of the communication system are provided to compare the set of achievable rates under different architecture designs and parameters. Circuit simulations and measurement results, based on both 22 nm FDSOI CMOS technology and 65 nm Bulk CMOS transistor technologies, are provided to justify the power efficiency of the proposed receiver architecture deploying envelope detectors and polynomial operators.

## I. INTRODUCTION

In order to accommodate the ever-growing demand for higher data-rates, the wireless spectrum has been continuously expanding over the past several decades. Particularly, millimeter wave (mm-wave) communication networks are being used in the fifth generation (5G) wireless systems to allow for larger channel bandwidths compared to earlier generation radio frequency (RF) systems which operate in frequencies below 6 GHz [3]. However, the energy consumption of components such as analog to digital converters (ADCs) increases significantly in mm-wave systems due to several factors as elaborated in the following. In theory, the power consumption of an ADC grows linearly with bandwidth, and the rate of increase is even more significant in practical implementations due to

the excessive loss associated with the passive components at higher frequencies, which causes an abrupt drop in ADC energy-efficiency as the bandwidth is pushed past 100 MHz [4]–[6]. For instance, the power consumption of current commercial high-speed ( $\geq 20$  GSamples/s), high-resolution (e.g. 8–12 bits) ADCs is around 500 mW per ADC [7]. Furthermore, in order to mitigate the inherent high isotropic path loss and sensitivity to blockages at high frequencies, mm-wave systems must leverage directive narrow-beams, by using large antenna arrays to increase the antenna gain at both base stations (BS) and user-ends (UE) [4], [8]–[10]. For instance, 5G wireless networks envision hundreds of antennas at the BS and in excess of ten antennas at the UE [11].

In conventional multiple-input multiple-output (MIMO) systems with digital beamforming, each antenna output is digitized separately by a dedicated ADC. This requires a large number of ADCs which are a significant source of power consumption in large bandwidth MIMO receivers [12], [13]. Analog and hybrid beamforming has been proposed as a way to mitigate ADC power consumption by reducing the number of ADCs. Under hybrid beamforming, the receiver terminals use a collection of analog beamformers to linearly combine the large number of received signals and feed them to a small set of ADCs. Additionally, in standard ADC design, power consumption is proportional to the number of quantization bins and hence grows exponentially in the number of output bits [14], which prohibits the use of high resolution ADCs.

There has been extensive recent efforts to design receiver architectures and coding strategies using analog, hybrid, and digital beamforming with a small number of few-bit ADCs [12], [15]–[26]. One method that has been proposed is to use digital beamforming architectures using one-bit ADCs [27]. A limitation of this approach is that digital beamforming requires an ADC per receiver antenna (two ADCs if input is considered in the complex domain), which leads to high power consumption. Furthermore, the restriction to one-bit ADCs may be prohibitively costly in terms of achievable rates. To mitigate this, hybrid beamforming has been proposed as an alternative approach. In hybrid beamforming, the receiver terminals in MIMO systems use a set of analog beamformers in the RF domain to combine the large number of analog signals at the receiver antennas and feed them to a small set of ADCs [12], [18], [19], [28]. Hybrid beamforming uses simple analog processing, linear processing in particular, to partially mitigate the rate loss due to low resolution quantization. In [29] a

This work was presented in part at 2022 IEEE International Symposium on Information Theory [1], and 2022 IEEE Global Communications Conference [2]. This work was supported in part by NSF grants CCF-2241057 and CCSS-2242700/2233783.

power-efficient hybrid MIMO receiver is presented where the analog and digital processing are jointly optimized by using task-specific quantization techniques. The hybrid beamforming approach was further extended in [30], where the use of hybrid blockwise architectures, consisting of delay elements, was considered. This allows for temporal linear processing of the received signals in the analog domain, providing additional degrees of freedom in choosing the processing function. Additionally, adaptive thresholds ADCs, were considered in [30], which allow for modifying the ADC thresholds based on past quantization outputs. This has similarities with the operation of successive approximation register (SAR) ADCs [31], [32]. The latter two approaches improve the channel capacity compared with that of the conventional hybrid beamforming architectures, however, the practical implementation of high precision analog delay elements, and SAR ADCs with high sampling rates is challenging due to synchronization issues and delay accuracy limitations.

In this work, we argue that the aforementioned digital, hybrid, and analog beamforming approaches suffer from the curse of low dimensions phenomenon, elaborated on in Section III. We further quantify the rate-loss due to this phenomenon, and provide solutions to mitigate it. Particularly, we consider the use of nonlinear analog operators — such as envelope detectors and low degree polynomial operators — prior to sampling and quantization, as a way to mitigate the rate-loss due to coarse quantization and increase channel capacity of MIMO systems with few-bit ADCs. The power consumption and circuit design for receiver architectures deploying these nonlinear operators based on measurement and simulation results in 22 nm and 65 nm CMOS technologies are provided in Section VIII.

The main contributions of this work are summarized below:

- To characterize the channel capacity under analog beamforming when envelope detectors are used for analog signal processing. The capacity expression is derived in terms of the power budget for analog processing components and ADCs, which in turn determines the number of ADCs,  $n_q$ , number of output levels of each ADC,  $\ell$ , and number of concatenated envelope detectors,  $\delta_{env}$  (Theorems 1-3).
- To characterize the high SNR capacity under analog beamforming when polynomial operators are used for analog signal processing. The high SNR capacity and inner-bounds to the low SNR achievable rates are provided in terms of the power budget of analog processing components and the ADCs, which in turn determine the number of ADCs,  $n_q$ , number of output levels of each ADC,  $\ell$ , and the polynomial degree,  $\delta_{poly}$  (Theorem 4).
- To provide a receiver architecture for hybrid beamforming using envelope detectors for high data rate communication with QAM demodulation (Theorem 5).
- To provide computational methods for finding the set of achievable rates and quantifying the gains due to nonlinear analog processing under the proposed analog and hybrid beamforming architectures, and to provide explanations of how these gains change as SNR,  $n_q$ ,  $\ell$ , and  $\delta$  are changed.
- To provide circuit designs and associated performance simulations for implementing polynomials of degree up to four

and concatenated envelope detector sequences with a pair of envelope detectors, and to evaluate their power consumption.

The organization of the remainder of the paper is as follows: In Section II, we provide an overview of prior works under both digital and hybrid beamforming and elaborate on the motivation behind considering nonlinear processing in the analog domain. We provide several motivating examples to illustrate the curse of low dimensions phenomenon and motivate the use of non-linear analog operators in Section III. In Section IV, we consider the scenario where the set of implementable analog processing functions consists of those generated by collections of envelope detectors, and propose receiver architectures, design coding strategies, and derive the fundamental performance limits in terms of achievable rates. In Section V, we study receiver architectures and coding strategies associated with analog polynomial operators. In Section VI, we consider a hybrid beamforming architecture that is equipped with envelope detectors. We provide achievable rates under this architecture in a high SNR regime. A numerical analysis for channel capacity with respect to each of the described architectures is provided in Section VII. Here we characterize the gains that result from the use of nonlinear processing in the analog domain. Transceiver Circuit designs and simulations evaluating the power consumption of the nonlinear processing operators including sequences of concatenated envelope detectors and polynomial operators are provided in Section VIII.

*Notation:* Upper-case letters such as  $X, \mathbf{Y}, \mathbf{H}$  are used to represent random variables, vectors, and matrices, and lower-case letters such as  $x, \mathbf{y}, \mathbf{h}$  represent their realizations. The set  $\{1, 2, \dots, n\}, n \in \mathbb{N}$  is represented by  $[n]$ . The vector  $(x_1, x_2, \dots, x_n)$  is written as  $x(1:n)$  and  $x^n$ , interchangeably, and  $(x_k, x_{k+1}, \dots, x_n)$  is denoted by  $x(k:n)$ . The  $i$ th element is written as  $x(i)$  and  $x_i$ , interchangeably. We write  $\|\cdot\|_2$  to denote the  $L_2$ -norm. An  $n \times m$  matrix is written as  $h(1:n, 1:m) = [h_{i,j}]_{i,j \in [n] \times [m]}$ , its  $i$ th column is  $h(:, i), i \in [m]$ , and its  $j$ th row is  $h(j, :), j \in [m]$ . We write  $\mathbf{x}$  and  $\mathbf{h}$  instead of  $x(1:n)$  and  $h(1:n, 1:m)$ , respectively, when the dimension is clear from context. The notation  $\mathbf{x}^H$  is used to denote the hermitian of  $\mathbf{x}$ . Sets are denoted by calligraphic letters such as  $\mathcal{X}$ , families of sets by sans-serif letters such as  $X$ , and collections of families of sets by  $\mathcal{X}$ .

## II. PRELIMINARIES

### A. The Classical Information Theoretic MIMO Communications Model

The classical model for Point-to-Point (PtP) MIMO communications is shown in Figure 1(a). The model has been considered under various scenarios such as availability of channel state information (CSI) at one or both terminals, time-varying channels, and lossy transmission of sources over MIMO channels, e.g., [33], [34]. A consequential idealization in the classical model is that no restrictions are imposed on the choice of encoding and decoding functions  $g(\cdot)$  and  $f(\cdot)$  at the transmitter and receiver terminals, respectively. At the receiver side, the justification is that the decoding function may be implemented by first constructing a faithful digital

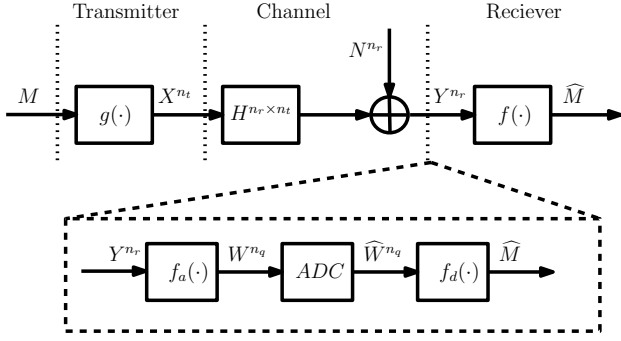


Fig. 1. MIMO system  $n_t$  transmit antennas,  $n_r$  receive antennas, and  $n_q$  ADCs. The receiver model (dashed box) consists of analog processing  $f_a(\cdot)$ , analog to digital conversion (ADC), and digital processing  $f_d(\cdot)$  modules.

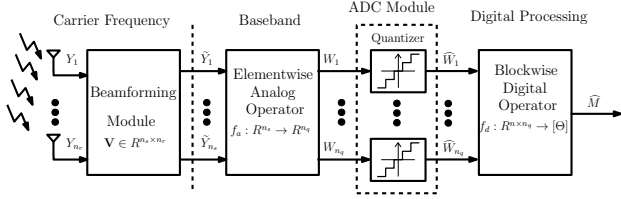


Fig. 2. The receiver architecture consists of an analog/hybrid beamforming module, an elementwise analog operator  $f_a(\cdot)$ ,  $n_q$  low-resolution ADCs, and a blockwise digital operator  $f_d(\cdot)$  with blocklength  $n$ .  $Y$  represents the received signal,  $\hat{M}$  is the message reconstruction, and  $[\Theta]$  is the message set.

representation of the analog signal using high resolution ADCs and then performing a blockwise decoding operation on these signals in the digital domain. However, this idealistic model does not capture the limitations on the resolution of the ADCs and the limitations of analog circuit design in mm-wave systems mentioned in the introduction. In this work, we focus on the receiver side, and consider a system model which captures the aforementioned practical considerations in the receiver architecture.

We consider a MIMO channel whose input and output<sup>1</sup>  $(\mathbf{X}, \mathbf{Y}) \in \mathbb{R}^{n_t} \times \mathbb{R}^{n_r}$  are related through  $\mathbf{Y} = \mathbf{h}\mathbf{X} + \mathbf{N}$ , where,  $\mathbf{h} \in \mathbb{R}^{n_r \times n_t}$  is the (fixed) channel matrix,  $n_t$  is the number of transmit antennas,  $n_r$  is the number of receive antennas, and  $\mathbf{N} \in \mathbb{R}^{n_r}$  is a jointly Gaussian noise vector. The channel input has average power constraint  $P_T$ , i.e.  $\mathbb{E}(\|\mathbf{X}\|_2^2) \leq P_T$ , where  $\|\cdot\|_2$  denotes the  $\ell_2$  distance. The receiver model is shown in Figure 1. The model encompasses the analog beamforming, hybrid beamforming, and digital beamforming models used in prior works as well as the beamforming models introduced in the subsequent sections. As observed from the figure, the choice of the decoding function at the receiver is restricted by limitations on the number of ADCs,  $n_q \in \mathbb{N}$  — which is in turn restricted by the power budget at the receiver side — and the set of *implementable nonlinear analog functions*  $f_a(\cdot)$ . In general, we assume that the analog function  $f_a(\cdot)$  is chosen from a predefined set of implementable functions  $\mathcal{F}_a$ . Each of these restrictions are elaborated on in the subsequent sections.

Formally, the receiver (Figure 2), consists of:

i) A beamforming module characterized by  $\mathbf{V} \in \mathbb{R}^{n_r \times n_r}$  which takes  $\mathbf{Y} \in \mathbb{R}^{n_r}$  as input and outputs  $\tilde{\mathbf{Y}} \in \mathbb{R}^{n_s} = \mathbf{V}\mathbf{Y}$  using a

collection of phase shifters.

ii) A set of elementwise analog processing functions  $f_j \in \mathcal{F}_a$ ,  $j \in [n_q]$ ,  $\delta \in \mathbb{N}$  operating on the beamformer output  $\mathbf{Y}$  to produce the vector  $W(1:n_q)$ , where  $W(j) = f_j(\mathbf{Y})$ ,  $j \in [n_q]$ . Note that both  $\mathbf{V}$  and  $f_a(\cdot)$  capture operations performed in the analog processing of the received signals. Although the two operators are implemented in different frequency bands — the carrier frequency and baseband, respectively — they can be effectively combined together into one module for the purpose of the derivations considered in this work. Consequently, in the following, we represent the analog processing module by  $f_a(\cdot)$ , and take  $\mathbf{V}$  as the identity matrix for conciseness. We consider two classes of analog linear processing functions:

**Concatenated Sequences of Envelope Detectors:** In Section IV, we consider the use of concatenated sequences of envelope detectors for analog signal processing. In this context, we define the set of implementable nonlinear analog functions as:

$$\mathcal{F}_{env}^\delta = \{f(y) = A_s(y, a^s), y \in \mathbb{R} | s \in [\delta], a^s \in \mathbb{R}^s\}, \quad \delta \in \mathbb{N},$$

where  $A_1(y, a) \triangleq |y - a|$ ,  $y, a \in \mathbb{R}$  and  $A_s(y, a^s) \triangleq A_1(A_{s-1}(y, a^{s-1}), a_s) = |A_{s-1}(y, a^{s-1}) - a_s|$ ,  $s \in \mathbb{N}$ . That is,  $\mathcal{F}_{env}^\delta$  consists of all functions which can be generated using sequences of  $s \leq \delta$  concatenated envelope detectors with thresholds  $a_1, a_2, \dots, a_s$ , respectively. The restriction to a limited number of envelope detectors is due to limitations in analog circuit design, and the implementability of such functions is justified by the circuit designs and simulations provided in Section VIII.

**Analog Polynomial Operators:** In Section V, we consider the use of polynomial operators. That is, we limit the set of implementable nonlinear analog functions to:

$$\mathcal{F}_{poly}^\delta \triangleq \{f(y) = \sum_{i=0}^{\delta} a_i y^i, y \in \mathbb{R} | a_i \in \mathbb{R}, i = 0, 1, \dots, \delta\}, \quad \delta \in \mathbb{N},$$

In this case,  $\mathcal{F}_{poly}^\delta$  consists of all polynomial functions of degree at most  $\delta$ , where the thresholds are determined by the roots of the polynomials. Similar to the case with envelope detectors, here the limitation on the degree of the polynomial functions is determined by limitations in the corresponding circuits design and is studied in Section VIII.

iii) A set of ADCs, whose number  $n_q$  and resolution<sup>2</sup>  $\ell$  is determined by a given power budget  $P_{ADC}$ . To elaborate, theoretically, the power consumption of an ADC is given by  $CVf_s 2^n$ , where  $C$  is the capacitive load,  $V$  is the voltage,  $f_s$  is the sampling frequency, and  $n$  is the number of output bits [35]. In our model, we define  $\alpha \triangleq CVf_s$ . As a result, if a one-bit ADC has a unit power consumption of  $\alpha$ , then an  $n$ -bit ADC has  $2^n \alpha$  power consumption. Consequently,  $n_q$  and  $\ell$  must belong to the set

$$\mathcal{N}(P_{ADC}) \triangleq \{(n_q, \ell) | \alpha n_q \ell \leq P_{ADC}\}.$$

The  $n_q$  ADCs have threshold vectors  $t(j, 1:\ell-1) \in \mathbb{R}^{\ell-1}$ ,  $j \in [n_q]$ , operating on the vector  $W(1:n_q)$  and producing  $\hat{W}(1:n_q)$

<sup>1</sup>To simplify notation, we have considered real-valued variables. The derivations can be extended to complex variables in a straightforward manner.

<sup>2</sup>Generally, one could assume different resolutions for each of the ADCs, however, we assume all ADCs have the same resolution to simplify the circuit design and implementation.

$n_q$ ), where

$$\widehat{W}(j) = k \quad \text{if} \quad W(j) \in [t(j, k), t(j, k + 1)], k \in [0, \ell - 1],$$

where  $j \in [n_q]$  and we have defined  $t(j, 0) \triangleq -\infty$  and  $t(j, \ell) \triangleq \infty$ . We call  $t(1:n_q, 1:\ell - 1)$  the *threshold matrix*. It is assumed that  $0 < t(i, j) < t(i, j'), i \in [n_q], j, j' \in [\ell - 1], j < j'$ <sup>3</sup>.

iv) A digital processing module represented by  $f_d : \{0, 1, \dots, \ell - 1\}^{n \times n_q} \rightarrow [\Theta]$ , operating on the block of ADC outputs after  $n$ -channel uses  $\widehat{W}(1:n, 1:n_q)$ . After the  $n$ th channel-use, the digital processing module produces the message reconstruction  $\widehat{M} = f_d(\widehat{W}(1:n, 1:n_q))$ . The communication system is characterized by  $(P_T, P_{ADC}, h, \delta)$ , and the transmission system by  $(n, n_q, \ell, \Theta, e, f^{n_q}, t(1:n_q, 1:\ell - 1), f_d)$ , where  $(n_q, \ell) \in \mathcal{N}(P_{ADC})$ ,  $f^{n_q} = (f_1, f_2, \dots, f_{n_q})$  and  $f_j \in \mathcal{F}_{env}^\delta, j \in [n_q]$ , and  $e(\cdot)$  is such that the channel input satisfies the average power constraint. Achievability and probability of error are defined in the standard sense. The capacity maximized over all implementable analog functions is denoted by  $C_{env}(P_T, P_{ADC}, h, \delta)$ , when using sequences of envelope detectors and by  $C_{poly}(P_T, P_{ADC}, h, \delta)$ , when using polynomial operators.

### B. Summary of Prior Works

In the following, we provide a brief summary of prior works on digital and hybrid beamforming, and explain how each scenario can be encompassed as a special case of the formulation described in the prequel.

**Prior Works on Digital Beamforming:** In digital beamforming, each antenna is directly connected to its dedicated ADC, i.e.,  $n_r = n_q$  and  $f_d(\cdot)$  is the identity function [36]–[40]. In [37], an approximate expression for the high signal-to-noise ratio (SNR) capacity of the single-input multiple-output (SIMO) system with digital beamforming was derived when one-bit ADCs are used; it was shown that the capacity is well-approximated by  $\log(4n_q + 1)$ . Note that *ideally*, one would expect that at high SNRs, when the channel is almost noiseless,  $n_q$  bits of information can be recovered per channel-use using  $n_q$  one-bit ADCs. It can be observed that there is a significant gap between the performance of the digital beamforming architecture ( $\log(4n_q + 1)$  bits/channel-use) and the ideal performance ( $n_q$  bits/channel-use). In this work, we argue that this gap is due to what we call the ‘*curse of low dimensions*’, further discussed in Section III and provide solutions to breach this performance gap.

**Prior Works on Hybrid Beamforming:** Hybrid beamforming architectures use a set of analog beamformers to linearly combine the received signals in the analog domain [19], [41], [42], i.e.,  $f_a(\cdot)$  is a linear function which can be captured by matrix  $\mathbf{V}^{n_q \times n_r}$  (Figure 3). This linear analog signal processing improves performance, in terms of achievable rates, by rotating the received signal such that the information-loss in the quantization step is reduced. For Gaussian SISO channels, hybrid beamforming with non-zero threshold ADCs was investigated in [43]. In MIMO communications, the use of analog linear combiners to reduce the quantization rate-loss was investigated

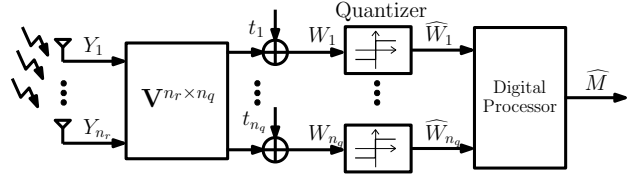


Fig. 3. The figure shows the hybrid beamforming architecture studied in prior works. The matrix  $\mathbf{V}^{n_r \times n_q}$  characterizes the analog linear combiner, and  $t^{n_q}$  is the vector of ADC thresholds.

in [19], [44]. Similar to the digital beamforming scenario alluded to above, the high SNR achievable rate in systems with hybrid beamforming has been shown to grow logarithmically in  $n_q$  [44]. This is significantly lower than the *ideal* high SNR performance of  $n_q$  bits/channel-use. Similar to digital beamforming, we argue that this loss in performance is due to the ‘*curse of low dimensions*’ and provide solutions to improve achievable rates.

**Prior Works on Analog Beamforming:** Analog beamforming utilizes analog phase shifters and only one RF chain for the beamforming operation [16], [45]. This leads to a simplified design and low power consumption compared to hybrid and digital beamforming. However, analog beamforming can only support single-stream transmission which yields lower data rates.

### III. CURSE OF LOW DIMENSIONS

As mentioned in Section II, in both the digital and hybrid beamforming scenarios studied in prior works, there is a rate-loss associated with the use of low-resolution ADCs even in the high SNR regime. That is, while ideally one would wish to achieve a communication rate of  $n_q$  bits per channel-use in the high SNR regime, in reality, the maximum achievable rate only grows logarithmically in the number of ADCs in both scenarios. In this section, we provide a high-level reasoning for this rate-loss. This intuitive explanation forms the motivation for the rest of the paper, and justifies the gains observed when using non-linear operators instead of linear operators as in hybrid beamforming schemes.

To explain the ‘*curse of low dimensions*’ phenomenon, let us consider a PtP MIMO system with hybrid beamforming at the receiver, operating in the high SNR regime, and consisting of  $n_t$  transmit antennas,  $n_r$  receive antennas, and  $n_q$  one-bit ADCs. Given a hybrid beamforming matrix  $\mathbf{V}$  and ADC threshold vector  $\mathbf{t}$ , one can define the quantization mapping  $Q(\mathbf{Y}) \triangleq \widehat{\mathbf{W}} = (\text{sign}(W_1), \text{sign}(W_2), \dots, \text{sign}(W_{n_q}))$ , where

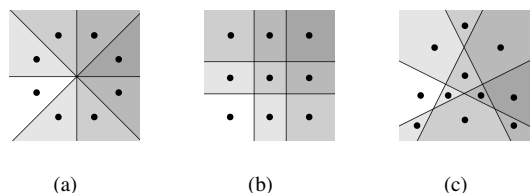


Fig. 4. Constellations resulting from linear processing prior to quantization in a scenario with  $n_t = n_r = 2$  and  $n_q = 4$ .

<sup>3</sup>Note that the assumption  $0 < t(i, j)$  does not lose generality since  $0 \leq |y|, \forall y \in \mathbb{R}$ . Hence, a negative threshold would yield trivial ADC output.

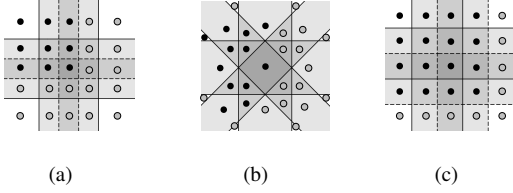


Fig. 5. Constellations resulting from nonlinear processing prior to quantization in a scenario with  $n_t = n_r = 2$  and  $n_q = 4$ .

$\mathbf{W} = \mathbf{V} + \mathbf{t}$ . An important characteristic of  $Q(\cdot)$  is the resulting Voronoi regions — where a Voronoi region  $\mathcal{P}$  is defined as the set of all vectors  $\mathbf{Y}$  which are mapped to the same quantization output. We let  $\mathcal{P} = \{\mathcal{P}_1, \mathcal{P}_2, \dots, \mathcal{P}_{|\mathcal{P}|}\}$  denote the set of all Voronoi regions of  $Q(\cdot)$ . In the high SNR regime, it is straightforward to argue that the number of messages which can be transmitted reliably per channel-use is equal to the number of Voronoi regions of  $Q(\cdot)$ , i.e., the maximum achievable rate is  $\log |\mathcal{P}|$  bits/channel-use. Ideally, the number of Voronoi regions grows exponentially with the number of one-bit ADCs (i.e.,  $|\mathcal{P}| = 2^{n_q}$ ) so that rate equal to  $n_q$  bits/channel-use is achieved. However, this is not the case for low-dimensional spaces where the maximum number of possible Voronoi regions produced by a mapping  $Q(\cdot)$  may be significantly lower than  $2^{n_q}$  [46]. In general, the maximum number of Voronoi regions is equal to the maximum number of regions in an  $n_r$ -dimensional space when cut by  $n_q$  hyperplanes [47], [48] given by:

$$|\mathcal{P}| = 2 \sum_{i=0}^{n_r-1} \binom{n_q-1}{i}. \quad (1)$$

Consequently, for a fixed  $n_r$ , the maximum achievable rate  $\log |\mathcal{P}|$  given with (1) grows logarithmically with  $n_q$ . Whereas if  $n_r = n_q$  (digital beamforming), then  $\log |\mathcal{P}|$  grows linearly in  $n_q$ . We call this phenomenon the *curse of low dimensions* since it leads to reduced rates when the channel output dimension is low, i.e., when  $n_r < n_q$ . This is further clarified through the following example.

**Example 1 (Curse of Low Dimensions).** *To provide a concrete example, let us consider a scenario with two transmit and receive antennas (i.e.  $n_t = n_r = 2$ ) and  $n_q = 4$  one-bit ADCs at the receiver. For ease of explanation, we focus on the achievable communication rates in the high SNR regime. In this case, the received signal space is a two-dimensional space consisting of points  $(Y_1, Y_2)$ . In hybrid beamforming, the received signals are passed through a linear analog combiner characterized by  $\mathbf{V} = [v_{i,j}]_{i,j \in [4]}$ , and the ADC thresholds are  $t_i \in \mathbb{R}, i \in [4]$ . The ADCs perform the following comparisons  $v_{i,1}Y_1 + v_{i,2}Y_2 \leq t_i, i \in [4]$ . The resulting Voronoi regions can be represented by a partition of the two-dimensional Euclidean space using four lines. For instance, in Phase-shift keying (PSK) modulation the thresholds are  $t_i = 0, i \in [4]$  and*

$$\begin{aligned} v_{1,1} &= 0, & v_{1,2} &= 1, & v_{2,1} &= -1, & v_{2,2} &= 1, \\ v_{3,1} &= 1, & v_{3,2} &= 0, & v_{4,1} &= 1, & v_{4,2} &= 1. \end{aligned}$$

The resulting Voronoi regions are shown in Figure 4(a). It can be observed that there are 8 Voronoi regions, as opposed to the ideal 16 regions. Alternatively, Figure 4(b) shows the Quadrature Amplitude Modulation (QAM) Voronoi regions, and Figure 4(c) represents a general position constellation proposed in [30], which achieves the highest number of Voronoi regions possible using analog linear processing. As was observed in [30], and shown in the figure, hybrid beamforming architectures can achieve at most 11 unique Voronoi regions thus achieving a rate of  $\log 11$  bits/channel-use.

An alternative approach is to use non-linear analog processing instead of the linear processing used in hybrid beamforming architectures. For instance, absolute values of the signals can be generated in the analog domain using envelope detectors, and then using the ADCs, the following comparisons can be made:

$$|\mathbf{Y}_1| \leq 1, \quad |\mathbf{Y}_2| \leq 1, \quad |\mathbf{Y}_1| \leq 3, \quad |\mathbf{Y}_2| \leq 3.$$

The resulting Voronoi regions from such processing are shown in Figure 5(a). The regions whose elements are associated with unique ADC binary output vectors are indicated with a black circular marker. Note that not all regions result in a unique ADC output. For example, if  $Y_i$  are very large positive numbers (top-right corner) or very large negative numbers (bottom-left corner), then the ADC outputs are  $(1, 1, 1, 1)$  for elements of both regions, hence only one of the two regions contributes to the achievable rate as it corresponds to a unique transmitted message. Similarly, the top-left and bottom-right regions produce ADC output  $(1, 1, 1, 1)$ . In the figure, we have marked the top-left region with a black circular marker, which indicates its contribution to the rate computation. Thus, the rate is not defined by the total number of quantization regions but by the number of unique regions. The constellation produces a total of 9 unique quantization regions, resulting in a rate of  $\log 9$  bits/channel use. Figure 5(b) shows a different set of Voronoi regions resulting from the following operations:

$$|\mathbf{Y}_1| \leq 1, \quad |\mathbf{Y}_2| \leq 1, \quad |\mathbf{Y}_1 + \mathbf{Y}_2| \leq 1, \quad |\mathbf{Y}_1 - \mathbf{Y}_2| \leq 1,$$

resulting in a rate of  $\log 12$  bits/channel use and the constellation in Figure 5(c) results from the operations:

$$|\mathbf{Y}_1| \leq 1, \quad |\mathbf{Y}_2| \leq 1, \quad |\mathbf{Y}_1 - 1| \leq 1, \quad |\mathbf{Y}_2 - 1| \leq 1,$$

which results in the optimal rate of 4 bits/channel use, thus completely lifting the curse of low dimensions.

#### IV. SISO SYSTEMS EQUIPPED WITH ENVELOPE DETECTORS

As discussed in the introduction, two different approaches, namely hybrid beamforming and low resolution quantization, have been proposed to address the ADC power consumption in wideband systems. In this section, as a first step, we consider single-input single-output (SISO) systems — modeling analog beamforming — equipped with low resolution ADCs and evaluate the achievable rate using non-linear analog processing, particularly, envelope detectors. This serves as a foundation for the derivations for hybrid beamforming in the subsequent sections. Hence, we consider a MIMO receiver with analog beamforming equipped with a collection of envelope detectors

for analog signal processing and a power budget of  $P_{ADC}$  for ADC power consumption. Our main objective in this section is to characterize the optimal values for the number and resolution of the ADCs used at the receiver terminal, which achieve the maximum system throughput, given the signal-to-noise ratio of the channel and the ADC power budget.

#### A. Envelope Detectors for Non-linear Analog Processing

Envelope detectors are suitable for analog processing of signals at high frequencies due to their low power consumption and simple circuit design [49]. The power consumption of envelope detectors is significantly lower at high data rates (see Section VIII). An envelope detector is parametrized by its threshold  $a \in \mathbb{R}$  and its operations on an input  $x \in \mathbb{R}$  are captured by the function  $A_1(x, a) = |x - a|, x \in \mathbb{R}$ . Envelope detectors can be concatenated in a sequence to generate a larger collection of analog operators. The operation of a sequence of  $s \in \mathbb{N}$  envelope detectors with bias vector  $a^s = (a_1, a_2, \dots, a_s)$  is captured by the iterative relation  $A_s(x, a^s) = |A_{s-1}(x, a^{s-1}) - a_s|, s > 1$ . It should be noted that concatenating large numbers of envelope detectors leads to increased circuit noise, and power consumption. Hence, there is a tradeoff between power-consumption, circuit complexity and robustness, and degrees of freedom in generating analog processing functions which in turn affects the set of achievable rates. This tradeoff is quantified in this section by deriving the set of achievable rates in terms of the number of concatenated envelope detectors.

#### B. Communication Strategies and Achievable Rates

In this section, we determine the optimal number and resolution of ADCs required at the receiver terminal to maximize system throughput, taking into consideration the signal-to-noise ratio of the channel and the ADC power budget. Additionally, we investigate the channel capacity for a given communication system, parametrized by  $(P_T, P_{ADC}, \mathbf{h}, \delta)$ .

**Definition 1 (Quantizer).** Given a threshold matrix  $\mathbf{t} \in \mathbb{R}^{n_q \times (\ell-1)}$  and functions  $f_j \in \mathcal{F}_{env}^\delta$ , a quantizer  $Q : \mathbb{R} \rightarrow [\ell]^{n_q}$  characterized by the tuple  $(\ell, \delta, n_q, \mathbf{f}^{n_q}, \mathbf{t})$  is defined as  $Q(\cdot) \triangleq (Q_1(\cdot), Q_2(\cdot), \dots, Q_{n_q}(\cdot))$ , where  $Q_j(y) \triangleq k$  if and only if  $f_j(y) \in [t(j, k), t(j, k+1)]$ ,  $j \in [n_q]$ . The associated partition of  $Q(\cdot)$  is:

$$\mathcal{P} = \{\mathcal{P}_i, \mathbf{i} \in [\ell]^{n_q}\} - \Phi, \text{ where } \mathcal{P}_i = \{y \in \mathbb{R} | Q(y) = \mathbf{i}\}, \mathbf{i} \in [\ell]^{n_q}.$$

For a quantizer  $Q(\cdot)$ , we call  $y \in \mathbb{R}$  a *point of transition* if the value of  $Q(\cdot)$  changes at input  $y$ , i.e. if it is a point of discontinuity of  $Q(\cdot)$ . Let  $r$  be a point of transition of  $Q(\cdot)$ . Then, there must exist output vectors  $\mathbf{c} \neq \mathbf{c}'$  and  $\epsilon > 0$  such that  $Q(y) = \mathbf{c}, y \in (r - \epsilon, r)$  and  $Q(y) = \mathbf{c}', y \in (r, r + \epsilon)$ . So, there exists  $j \in [n_q]$  and  $k \in [\ell - 1]$  such that  $f_j(y) < t(j, k), y \in (r - \epsilon, r)$  and  $f_j(y) \geq t(j, k), r \in (r, r + \epsilon)$ , or vice versa; so that  $r$  is a root of the function  $f_{j,k}(y) \triangleq f_j(y) - t(j, k)$ . Let  $r_1, r_2, \dots, r_\gamma$  be the sequence of roots of  $f_{j,k}(\cdot), j \in [n_q], k \in [\ell - 1]$  (including repeated roots), written in non-decreasing order, where  $\gamma \triangleq (\ell - 1)n_q 2^\delta$ . Let  $C = (\mathbf{c}_0, \mathbf{c}_1, \dots, \mathbf{c}_\gamma)$  be the corresponding quantizer outputs, i.e.  $\mathbf{c}_{i-1} = \lim_{y \rightarrow r_i^-} Q(y), i \in [\gamma]$  and  $\mathbf{c}_\gamma = \lim_{y \rightarrow \infty} Q(y)$ .

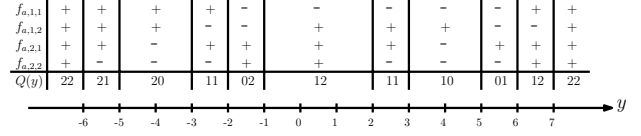


Fig. 6. The quantizer outputs in Example 2. The first four rows show the sign of the function  $f_{j,k}, j, k \in \{1, 2\}$  for the values of  $y$  within each interval. The last row shows the quantizer output in that interval.

We call  $C$  the *code* associated with the quantizer and it plays an important role in the analysis provided in the sequel. Note that the associated code is an ordered set of vectors. The size of the code  $|C|$  is defined as the number of unique vectors in  $C$ . Each  $\mathbf{c}_i = (c_{i,1}, c_{i,2}, \dots, c_{i,n_q}), i \in \{0, 1, \dots, \gamma\}$  is called a codeword. For a fixed  $j \in [n_q]$ , the transition count of position  $j$  is the number of codeword indices where the value of the  $j$ th element changes, and it is denoted by  $\kappa_j$ , i.e.,  $\kappa_j \triangleq \sum_{k=1}^{\gamma} \mathbb{1}(c_{i_{k-1},j} \neq c_{i_k,j})$ . It is straightforward to see that  $|\mathcal{P}| = |C|$  since both cardinalities are equal to the number of unique outputs the quantizer produces. The following example clarifies the definitions given above.

**Example 2 (Associated Code).** Let  $n_q = \delta = 2$  and  $\ell = 3$  and consider a quantizer characterized by analog processing functions  $f_1(y) = A_2(y, (2, 4)) = \|y - 2\| - 4|$  and  $f_2(y) = A_2(y, (4, 0)) = \|y - 4\|, y \in \mathbb{R}$ , and thresholds

$$t(1, 1) = 0, \quad t(1, 2) = 1, \quad t(2, 1) = 1, \quad t(2, 2) = 2,$$

We have:

$$f_{1,1}(y) = \|y - 2\| - 4| - 1, \quad f_{1,2}(y) = \|y - 2\| - 4|$$

$$f_{2,1}(y) = \|y - 4\| - 1, \quad f_{2,2}(y) = \|y - 4\| - 2.$$

The ordered root sequence is  $(r_1, r_2, \dots, r_{10}) = (-6, -5, -3, -2, -1, 2, 3, 5, 6, 7)$ . The associated partition is:

$$\mathcal{P} = \{[-\infty, -6), (-6, -5), (-5, -3), (-3, -2), (-2, -1), (-1, 2), (2, 3), (3, 5), (5, 6), (6, 7), (7, \infty)\}.$$

The associated code is given by 22, 21, 20, 11, 02, 12, 11, 10, 01, 12, 22. This is shown in Figure 6. The size of the code is  $|C| = 8$ . The high SNR capacity of a channel using this quantizer at the receiver is  $\log |\mathcal{P}| = \log |C| = \log 8$ .

1) *Single Envelope Detector and One-bit Quantization:* As a first step, we investigate scenarios with  $\ell = 2$  and  $\delta = 1$ . We will build upon this to derive capacity expressions for  $\delta, \ell \in \mathbb{N}$ . It can be noted that since  $\delta = 1$ , each  $f_j(y)$  is of the form  $|y - a_j|$  for some  $a_j \in \mathbb{R}$ . We sometimes write  $f_{a_j,j}(y) = |y - a_j|$  to explicitly denote the value of  $a_j$ . Given threshold  $t_j > 0$  the roots of  $f_{a_j,j}(y) - t_j$  are equal to  $a_j \pm t_j$ . The following proposition provides the high SNR capacity when  $\ell = 2, \delta = 1$ .

**Proposition 1 (High SNR SISO Capacity with One-bit ADCs and Single-level Envelop Detectors).** Let  $h \in \mathbb{R}, h \neq 0$ , and  $n_q > 1$ . Further assume that the ADC resolution is limited to  $\ell = 2$ . Then,

$$\lim_{P_T \rightarrow \infty} C_{env}(P_T, P_{ADC}, h, 1) = 1 + \log \left\lfloor \frac{P_{ADC}}{2\alpha} \right\rfloor,$$

where  $\alpha$  is the unit of power consumption for a one-bit ADC.

*Proof.* Please see Appendix A.  $\square$

The following theorem provides a computable expression for the capacity under general assumptions on channel SNR.

**Theorem 1 (SISO Capacity with One-bit ADCs and Single-level Envelope Detectors).** Consider a system parametrized by  $(P_T, P_{ADC}, h, \delta)$ , where  $P_T, P_{ADC} > 0, h \in \mathbb{R}, n_q > 1$ , and  $\delta = 1, \ell = 2$ . Then, the capacity is given by:

$$C_{\text{env}}(P_T, P_{ADC}, h, \delta) = \sup_{\mathbf{x} \in \mathbb{R}^{2n_q+1}} \sup_{P_X \in \mathcal{P}_X(P_T)} \sup_{\mathbf{t} \in \mathbb{R}^{2n_q}} I(X; \widehat{Y}), \quad (2)$$

where  $n_q = \frac{P_{ADC}}{2\alpha}$ ,  $\widehat{Y} = Q(hX + N)$ ,  $N \sim \mathcal{N}(0, 1)$ ,  $\mathcal{P}_X(P_T)$  is the set of probability distributions defined on  $\{x_1, x_2, \dots, x_{2n_q+1}\}$  such that  $\mathbb{E}(X^2) \leq P_T$ , and  $Q(y) = k$  if  $y \in [t_k, t_{k+1}]$ ,  $k \in \{1, \dots, 2n_q\}$  and  $Q(y) = 0$  if  $y > t_{2n_q}$  or  $y < t_1$ .

*Proof.* Please see Appendix B.  $\square$

2) *Low-resolution ADCs and Concatenated Sequences of Envelope Detectors:* Next, we consider systems with  $\delta > 1, \ell > 2$ . Recall that for  $\delta > 1$ , each  $f_j(y), j \in [n_q]$  is of the form  $f_j(y) = A_\delta(y, a_j^\delta) = |A_{\delta-1}(y, a_j^{\delta-1}) - a_{j,\delta}|$ , where  $A_1(y, a_{j,1}) = |y - a_{j,1}|$ . For tractability, we use the notation  $f_{a_j^\delta, j}(y) \triangleq A_\delta(y, a_j^\delta)$  to explicitly denote the bias vector  $a_j^\delta$  used for the  $j$ th analog function. The following example introduces the concept of degenerate bias vectors for a given threshold matrix  $\mathbf{t}$ .

**Example 3 (Degenerate Bias Vector).** Let  $n_q = 1, \ell = 3, \delta = 2$ , and consider the thresholds  $t_{1,1} = 1$  and  $t_{1,2} = 2$ . Given a bias vector,  $(a_1, a_2)$ , the associated analog function is  $f_{a_1^\delta, 1}(y) = \|y - a_1 - a_2\|$ . The ADC output is

$$Q(y) = \begin{cases} 0 & \text{if } \|y - a_1 - a_2\| < 1 \\ 1 & \text{if } 1 < \|y - a_1 - a_2\| < 2 \\ 2 & \text{if } 2 < \|y - a_1 - a_2\| \end{cases}$$

Note that if  $a_2 - 1 < 0$ , then this would be equivalent with:

$$Q(y) = \begin{cases} 0 & \text{if } |y - a_1| < 1 + a_2 \\ 1 & \text{if } 1 < |y - a_1| < 2 + a_2 \\ 2 & \text{if } 2 + a_2 < |y - a_1| \end{cases}$$

In this case, the second envelope detector does not affect the quantization process and can be omitted without change in quantizer output, i.e., the input to the corresponding absolute value is always positive, so it can be removed.

We call bias vectors  $a_j^\delta, j \in [n_q]$  which yield redundant envelope detectors, such as the one in Example 3, degenerate bias vectors. The following proposition characterizes the necessary and sufficient conditions for non-degeneracy of bias vectors.

**Proposition 2 (Non-Degenerate Bias Vectors).** Let the threshold vector corresponding to the  $j$ th ADC be  $t^{\ell-1}$ , where  $j \in [n_q]$ . The bias vector of the corresponding analog operator  $f_j(\cdot)$  is non-degenerate if and only if:

$$0 < t_1 + \sum_{i=2}^{\delta} (-1)^{b_i} a_i, \quad \forall b_i \in \{-1, 1\}. \quad (3)$$

The proof follows by noting that from definition  $0 < t_1 < t_2 < \dots < t_{\ell-1}$  so that Equation (3) guarantees  $0 < t_k + \sum_{i=2}^{\delta} (-1)^{b_i} a_i$  for all  $k \in [\ell - 1]$ , and is thus sufficient to ensure non-degeneracy. We will use the following notion of a fully-symmetric vector in deriving properties of roots of quantizers with non-degenerative bias vectors.

**Definition 2 (Fully-Symmetric Vector).** A vector  $\mathbf{b} = (b_1, b_2, \dots, b_{2^n})$  is called symmetric if  $b_i + b_{2^n-i} = b_j + b_{2^n-j}, i, j \in [2^n - 1]$ .  $\mathbf{b}$  is called fully-symmetric if it is symmetric and the vectors  $(b_1, b_2, \dots, b_{2^{n-1}})$  and  $(b_{2^{n-1}+1}, b_{2^{n-1}+2}, \dots, b_{2^n})$  are both fully-symmetric for  $n > 2$  and symmetric for  $n = 2$ .

For instance, the vector  $\mathbf{b} = (-7, -6, -5 - 4, 4, 5, 6, 7)$  is fully symmetric since it is symmetric and  $(-7, -6, -5 - 4)$  and  $(4, 5, 6, 7)$  are both symmetric. As observed in previous section, the number and shape of the quantization Voronoi regions depends on the roots of the analog processing function. The following proposition characterizes useful properties of the roots which are used in the subsequent sections to derive capacity expressions of various communication systems.

**Proposition 3 (Properties of Roots of Associated Analog Functions).** Consider a quantizer  $Q(\cdot)$  with threshold matrix  $\mathbf{t} \in \mathbb{R}^{n_q \times (\ell-1)}$ , and analog processing functions  $f_j(\cdot), j \in n_q$ , such that the corresponding bias vectors are non-degenerate and  $f_{j,k}(\cdot) \triangleq f_j(\cdot) - t(j, k), j \in [n_q], k \in [\ell - 1]$  do not have repeated roots. Let  $r_1, r_2, \dots, r_\gamma$  be the increasing sequence of roots, where  $\gamma \triangleq (\ell - 1)n_q 2^\delta$ . Then, there exists a partition  $\{\mathcal{P}_{j,k}, j \in [n_q], k \in [\ell - 1]\}$  of  $[\gamma]$  such that

- 1)  $|\mathcal{P}_{j,k}| = 2^\delta, j \in [n_q], k \in [\ell - 1]$ .
- 2) For  $j \in [n_q], k \in [\ell - 1]$ , let  $\mathcal{P}_{j,k} = \{i_1, i_2, \dots, i_{2^\delta}\}$ , where  $i_j < i_{j'}$  for  $j < j'$ . The vector  $(r_{i_1}, r_{i_2}, \dots, r_{i_{2^\delta}})$  is fully-symmetric,
- 3) For all  $j \in [n_q], k, k' \in [\ell - 1]$ , we have  $r_{i_i} - r'_{i'_i} = r_{i'_i} - r'_{i'_i}, i_i, i'_i \in [2^\delta]$ , where  $r_{i_i}, r'_{i'_i} \in \mathcal{P}_{j,k}$  and  $r'_{i'_i}, r'_{i'_i} \in \mathcal{P}_{j,k'}$ .

The proof follows by taking each  $\mathcal{P}_{j,k}$  to be the ordered set of roots of  $f_{j,k}$  for a given  $j \in [n_q], k \in [\ell - 1]$  and using properties of the absolute value. The following proposition states several useful properties for the code associated with a quantizer  $Q(\cdot)$ .

**Proposition 4 (Properties of the Associated Code).** Consider a quantizer  $Q(\cdot)$  with threshold matrix  $\mathbf{t} \in \mathbb{R}^{n_q \times (\ell-1)}$  such that  $0 < t(i, j) < t(i, j'), i \in [n_q], j, j' \in [\ell - 1], j < j'$ , and analog processing functions  $f_j(\cdot), j \in n_q$ , such that the corresponding bias vectors are non-degenerate and  $f_{j,k}(\cdot) \triangleq f_j(\cdot) - t(j, k), j \in [n_q], k \in [\ell - 1]$  do not have repeated roots. The associated code  $\mathcal{C}$  satisfies the following:

- 1) The number of codewords in  $\mathcal{C}$  is equal to  $\gamma \triangleq (\ell - 1)n_q 2^\delta + 1$ , i.e.  $\mathcal{C} = (\mathbf{c}_0, \mathbf{c}_1, \dots, \mathbf{c}_{\gamma-1})$ .
- 2) All elements of the first codeword  $\mathbf{c}_0$  are equal to  $\ell - 1$ , i.e.  $c_{i,0} = \ell - 1, i \in \{0, 1, \dots, \gamma - 1\}$ .
- 3) Consecutive codewords differ in only one position, and their  $L_1$  distance is equal to one, i.e.  $\sum_{j=1}^{n_q} |c_{i,j} - c_{i+1,j}| = 1, i \in \{0, 1, \dots, \gamma - 1\}$ .
- 4) The transition count at every position is  $\kappa_j = \frac{\gamma}{n_q} = (\ell - 1)2^\delta, j \in [n_q]$ .
- 5) Let  $i_1, i_2, \dots, i_\kappa$  be the non-decreasingly ordered indices of codewords, where the  $j$ th element has value-transitions.

Then, the sequence  $(c_{i_1,j}, c_{i_2,j}, \dots, c_{i_\ell,j})$  is periodic, in each period it takes all values between 0 and  $\ell - 1$ , and  $|c_{i_k,j} - c_{i_{k+1},j}| = 1, k \in [k-1]$  holds. Furthermore,  $c_{i_1,j} \in \{0, \ell - 1\}$ .  
 6)  $|C| \leq \min(\ell^{n_q}, (\ell - 1)n_q 2^\delta)$ .

Proposition 4 is an extension of the properties shown in the proof of Theorem 1. We provide a brief justification of each property in the following. Property 1 follows by the fact that the number of codewords in  $C$  is equal to the number of roots of  $f_{j,k}, j \in [n_q], k \in [\ell - 1]$  plus one (e.g., see Figure 6). Property 2 and 6 follow by a similar argument as Equation (9) in proof of Proposition 1. Properties 3 and 5 follow by the fact that each root of  $f_{j,k}, j \in [n_q], k \in [\ell - 1]$  corresponds to a value transition in the output of exactly one of the ADCs (since the roots are not repeated) and at each transition the value changes either one unit up or down since in the input crosses one threshold at a time at its value is changed continuously. Property 4 follows by the fact that the transition count at each position is equal to the number of roots of  $f_{j,k}, k \in [\ell - 1]$  for a fixed  $j \in [n_q]$ .

As a step towards characterizing capacity when  $\ell > 2, \delta > 1$ , we first study the capacity region for systems with one-bit ADCs, i.e.,  $\ell = 2, \delta > 1$ . To this end, we prove two useful propositions. The first one shows that given an ordered set  $C$  satisfying the properties in Proposition 4 and a sequence of real numbers  $(r_1, r_2, \dots, r_\gamma)$  satisfying the properties in Proposition 3, one can always construct a quantizer whose associated code is equal to  $C$  and whose roots sequence is  $(r_1, r_2, \dots, r_\gamma)$ . The second proposition provides conditions under which there exists a code satisfying the properties in Proposition 4. The proof ideas follow techniques used in study of balanced and locally balanced gray codes [50], [51]. Combining the two results allows us to characterize the necessary and sufficient conditions for existence of quantizers with desirable properties.

In the statement of the following proposition, for a given code  $C$ , we have used the notation  $\xi_1, \xi_2, \dots, \xi_{\gamma-1}$  for the transition sequence of  $C$ . That is,  $\xi_k, k \in \{1, \dots, \gamma - 1\}$  is the bit position which is different between  $\mathbf{c}_{k-1}$  and  $\mathbf{c}_k$ . We have defined the transition sets  $\mathcal{I}_j \triangleq \{s | \xi_s = j\}, j \in [n_q]$ . Note from Property 5) in Proposition 4, we have  $|\mathcal{I}_j| = \kappa_j = 2^\delta$ .

**Proposition 5 (Quantizer Construction).** *Let  $\ell = 2, n_q \in \mathbb{N}$  and  $\delta > 1$  and consider an ordered set  $C \subset \{0, 1\}^{n_q}$  satisfying properties 1)-5) in Proposition 4, and a sequence of increasing real numbers  $r_1, r_2, \dots, r_\gamma$ , where  $\gamma = n_q 2^\delta$ , such that  $(r_i, s \in \mathcal{I}_j)$  is fully-symmetric for all  $j \in [n_q]$ , where  $\mathcal{I}_j$  are the transition sets of  $C$ . Then, there exists a quantizer  $Q(\cdot)$  with associated analog functions  $f_j(\cdot), j \in [n_q]$  such that its associated code is  $C$ , and  $r_1, r_2, \dots, r_\gamma$  is the non-decreasing sequence of roots of its associated analog functions  $f_{j,k}(\cdot), j \in [n_q], k \in [\ell - 1]$ .*

*Proof.* Please see Appendix C.  $\square$

**Proposition 6. (Code Construction)** *Let  $\ell = 2, n_q \in \mathbb{N}$ , and  $\kappa_1, \kappa_2, \dots, \kappa_{n_q}$  be even numbers such that  $|\kappa_j - \kappa_{j'}| \leq 2, j, j' \in [n_q]$ . Then, there exists a code  $C$  with transition count at position  $j$  equal to  $\kappa_j, j \in [n_q]$  satisfying properties 1), 2), 3), and 5) in Proposition 4 such that  $|C| = \min\{2^{n_q}, \sum_{j=1}^{n_q} \kappa_j\}$ . Particularly, if*

$\kappa_j = 2^\delta, j \in [n_q]$ , then there exists  $C$  with  $|C| = \min\{2^{n_q}, n_q 2^\delta\}$  satisfying properties 1)-5) in Proposition 4.

*Proof.* Please see Appendix D.  $\square$

Using Propositions 5 and 6, we characterize the channel capacity for  $\ell = 2$  and  $\delta > 1$ . Let us define  $\Gamma_2(n_q, \ell) \triangleq \min(2^{n_q}, n_q 2^\delta + 1)$  and the set  $\mathcal{T}_{\Gamma_2} \subseteq \mathbb{R}^{\Gamma_2-1}$  as the set of sequences of increasing real numbers  $r_1, r_2, \dots, r_\gamma$ , where  $\gamma = n_q 2^\delta$  for which there exists a partition  $\{\mathcal{I}_j, j \in [n_q]\}$  of  $[\delta]$  such that  $(r_i, s \in \mathcal{I}_j)$  is fully-symmetric for all  $j \in [n_q]$ , and there exists a code satisfying Properties 1)-5) in Proposition 4 whose transition sets are equal to  $\mathcal{I}_j, j \in [n_q]$  and which has exactly one repeated codeword, i.e., only the first and last codewords are repeated. The following theorem characterizes the channel capacity.

**Theorem 2 (SISO Capacity with One-bit ADCs and Multi-level Envelope Detectors).** *Consider a system parametrized by  $(P_T, P_{ADC}, h, \delta)$ , where  $P_T, P_{ADC} > 0, h \in \mathbb{R}, \delta > 1$ , and assume that the ADC resolution is restricted to  $\ell = 2$ . Then, the capacity is given by:*

$$C_{env}(P_T, P_{ADC}, h, \delta) = \max_{\substack{\gamma = \Gamma_2(n_q, \ell) \\ (n_q, \ell) \in \mathcal{N}(P_{ADC})}} \sup_{\mathbf{x} \in \mathbb{R}^\gamma} \sup_{P_{\mathbf{x}} \in \mathcal{P}_{\mathbf{x}}(P_T)} \sup_{t \in \mathcal{T}_\gamma} I(X; \widehat{Y}), \quad (4)$$

where  $\widehat{Y} = Q(hX + N)$ ,  $N \sim \mathcal{N}(0, 1)$ ,  $\mathcal{P}_{\mathbf{x}}(P_T)$  is the set of distributions on  $\{x_1, x_2, \dots, x_\gamma\}$  such that  $\mathbb{E}(X^2) \leq P_T$ , and  $Q(y) = k$  if  $y \in [t_k, t_{k+1}), k \in \{1, \dots, \gamma - 1\}$  and  $Q(y) = 0$  if  $y > t_{\gamma-1}$  or  $y < t_1$ .

The proof follows by similar arguments as in the proof of Theorem 1. The converse follows from Proposition 4 Item 4). Achievability follows from Proposition 6.

The region given in Theorem 2 is difficult to analyze since finding the set  $\mathcal{T}_\gamma$  may be computationally complex. Inner bounds to the achievable region may be numerically derived by assuming additional symmetry restriction such as uniform quantization restrictions. This is studied in more detail in the numerical evaluations provided in Section VII.

For scenarios with  $\ell > 2$  and  $\delta > 1$ , let us define  $\Gamma_\ell \triangleq \min(\ell^{n_q}, (\ell - 1)n_q \ell^\delta + 1)$  and the set  $\mathcal{T}_{\Gamma_\ell} \subseteq \mathbb{R}^{\Gamma_\ell-1}$  as the set of sequences of increasing real numbers  $r_1, r_2, \dots, r_\gamma$  satisfying the properties in Proposition 3, for which there exists a code  $C$  satisfying Properties 1)-5) in Proposition 4 such that i) the sets  $\mathcal{P}_{j,k}, j \in [n_q], k \in [\ell - 1]$  in 3) are the indices of the codewords of  $C$  which have transition to or from value  $k$  in their  $j$ th element, and ii)  $C$  has exactly one repeated codeword, i.e., only the first and last codewords are repeated. The following theorem characterizes the channel capacity. The proof follows from Propositions 4 and 6 similar to the arguments given in the proof of Theorem 1.

**Theorem 3 (SISO Capacity with Few-bit ADCs and Multi-level Envelope Detectors).** *Consider a system parametrized by  $(P_T, P_{ADC}, h, \delta)$ , where  $P_T, P_{ADC} > 0, h \in \mathbb{R}$ , and  $\delta \in \mathbb{N}$ . Let  $\Gamma_\ell, \ell \in \mathbb{N}$  be the maximum size of codes satisfying condition*



1)-5) in Proposition 4. Then,

$$C_{env}(P_T, P_{ADC}, h, \delta) = \max_{\substack{\gamma=\Gamma_\ell(n_q, \ell): \\ (n_q, \ell) \in \mathcal{N}(P_{ADC})}} \sup_{\mathbf{x} \in \mathbb{R}^\gamma} \sup_{P_X \in \mathcal{P}_X} \sup_{\mathbf{t} \in \mathcal{T}_\gamma} I(X; \widehat{Y}), \quad (5)$$

where  $\widehat{Y} = Q(hX + N)$ ,  $N \sim \mathcal{N}(0, 1)$ ,  $\mathcal{P}_X(P_T)$  consists of distributions on  $\{x_1, x_2, \dots, x_\gamma\}$  such that  $\mathbb{E}(X^2) \leq P_T$ , and  $Q(y) = k$  if  $y \in [t_k, t_{k+1}]$ ,  $k \in [\gamma - 1]$  and  $Q(y) = 0$  if  $y > t_{\gamma-1}$  or  $y < t_1$ .

Optimizing (5) requires calculating  $\Gamma_\ell(n_q, \ell)$ . The total number of codes satisfying conditions 1)-5) in Proposition 4 is bounded from above by  $\binom{(\ell-1)2^\delta n_q}{(\ell-1)2^\delta, (\ell-1)2^\delta, \dots, (\ell-1)2^\delta}$ . Hence, for systems with a few low-resolution ADCs and small  $\delta$  ( $\delta = 1, 2$ ), one can find  $\Gamma_\ell(n_q, \ell)$  by searching over all such codes.

## V. SISO SYSTEMS WITH POLYNOMIAL OPERATORS

In the previous section, we investigated the channel capacity for SISO systems (analog beamforming) when sequences of concatenated envelope detectors are used for analog signal processing. In this section, we evaluate the resulting channel capacity when analog polynomial operators are used instead of envelope detectors.

**Example 4 (Associated Code).** Let  $n_q = \delta = 2$  and  $\ell = 3$  and consider a quantizer characterized by polynomials  $f_{a,1}(y) = y^2 + 2y$  and  $f_{a,2}(y) = y^2 + 3y$ ,  $y \in \mathbb{R}$ , and thresholds

$$t(1, 1) = 3, \quad t(1, 2) = 0, \quad t(2, 1) = 10, \quad t(2, 2) = 18,$$

We have:

$$\begin{aligned} f_{a,1,1}(y) &= y^2 + 2y - 3, & f_{a,1,2}(y) &= y^2 + 2y \\ f_{a,2,1}(y) &= y^2 + 3y - 10, & f_{a,2,2}(y) &= y^2 + 3y - 18. \end{aligned}$$

The ordered root sequence is  $(r_1, r_2, \dots, r_8) = (-6, -5, -3, -2, 0, 1, 2, 3)$ . The associated partition is:

$$\mathbf{P} = \left\{ [-\infty, -6), (-6, -5), (-5, -3), (-3, -2), (-2, 0), (0, 1), (1, 2), (2, 3), (3, \infty) \right\}.$$

The associated code is given by 22, 21, 20, 10, 00, 10, 20, 21, 22. The size of the code is  $|C| = 5$ . The high SNR capacity of a channel using this quantizer at the receiver is  $\log|\mathbf{P}| = \log|C| = \log 5$ .

As a first step, we show the following proposition about properties of codes and their associated polynomial functions which is analogous to Proposition 4 which addressed codes and their associated envelope-detector-based analog processing functions. The proof follows by similar arguments as that of Proposition 4 and is omitted for brevity.

**Proposition 7 (Properties of Code and Associated Polynomial Functions).** Consider a quantizer  $Q(\cdot)$  with threshold matrix  $\mathbf{t} \in \mathbb{R}^{n_q \times (\ell-1)}$  and associated polynomials  $f_j(\cdot) \in \mathcal{F}_{poly}^\delta$ ,  $j \in n_q$ , such that  $f_{j,k}(\cdot) \triangleq f_j(\cdot) - t(j, k)$ ,  $j \in [n_q]$ ,  $k \in [\ell-1]$  do not have repeated roots. The associated code  $C$  satisfies the following:

- 1) The number of codewords in  $C$  is equal to  $\gamma \triangleq (\ell-1)\delta n_q + 1$ , i.e.  $C = (\mathbf{c}_0, \mathbf{c}_1, \dots, \mathbf{c}_{\gamma-1})$ .

- 2) All elements of the first codeword  $\mathbf{c}_0$  are either equal to  $\ell - 1$  or equal to 0, i.e.  $c_{i,0} = 0$ ,  $i \in \{0, 1, \dots, \gamma - 1\}$  or  $c_{i,0} = \ell - 1$ ,  $i \in \{0, 1, \dots, \gamma - 1\}$ .
- 3) Consecutive codewords differ in only one position, and their  $L_1$  distance is equal to one, i.e.  $\sum_{j=1}^{n_q} |c_{i,j} - c_{i+1,j}| = 1$ ,  $i \in \{0, 1, \dots, \gamma - 1\}$ .
- 4) The transition count at every position is  $\kappa_j = \frac{\gamma}{n_q} = (\ell - 1)\delta$ ,  $j \in [n_q]$ .
- 5) Let  $i_1, i_2, \dots, i_k$  be the non-decreasingly ordered indices of codewords where the  $j$ th element has value-transitions. Then, the sequence  $(c_{i_1,j}, c_{i_2,j}, \dots, c_{i_k,j})$  is periodic, in each period it takes all values between 0 and  $\ell - 1$ , and  $|c_{i_k,j} - c_{i_{k+1},j}| = 1$ ,  $k \in [k - 1]$  holds. Furthermore,  $c_{i,j} \in \{0, \ell - 1\}$ .
- 6) If  $\delta$  is even, then  $|C| \leq \min(\ell^{n_q}, (\ell - 1)\delta n_q)$  and if  $\delta$  is odd, then  $|C| \leq \min(\ell^{n_q}, (\ell - 1)\delta n_q + 1)$ .

Using Proposition 6 and Proposition 7, and following the arguments in the proof of Theorem 2, one can prove the following theorem.

**Theorem 4 (SISO Capacity with Few-bit ADCs and Polynomial Analog Operators).** Consider a system parametrized by  $(P_T, P_{ADC}, h, \delta)$ , where  $P_T, P_{ADC} > 0$ ,  $h \in \mathbb{R}$ , then for even-valued  $\delta$ , we have:

$$C_{poly}(P_T, P_{ADC}, h, \delta) = \max_{\substack{\gamma=\Gamma(n_q, \ell): \\ (n_q, \ell) \in \mathcal{N}(P_{ADC})}} \sup_{\mathbf{x} \in \mathbb{R}^\gamma} \sup_{P_X \in \mathcal{P}_X(P_T)} \sup_{\mathbf{t} \in \mathbb{R}^{\gamma-1}} I(X; \widehat{Y}), \quad (6)$$

and for odd-valued  $\delta$ , we have:

$$\begin{aligned} \max_{\substack{\gamma=\Gamma(n_q, \ell): \\ (n_q, \ell) \in \mathcal{N}(P_{ADC})}} \sup_{\mathbf{x} \in \mathbb{R}^\gamma} \sup_{P_X \in \mathcal{P}_X(P_T)} \sup_{\mathbf{t} \in \mathbb{R}^{\gamma-1}} I(X; \widehat{Y}) &\leq C_Q(P_T, P_{ADC}, h, \delta) \\ &\leq \max_{\substack{\gamma'=\Gamma'(n_q, \ell): \\ (n_q, \ell) \in \mathcal{N}(P_{ADC})}} \sup_{\mathbf{x} \in \mathbb{R}^{\gamma'}} \sup_{P_X \in \mathcal{P}_X(P_T)} \sup_{\mathbf{t} \in \mathbb{R}^{\gamma'-1}} I(X; \widehat{Y}), \end{aligned} \quad (7)$$

where  $n_q = \frac{P_{ADC}}{2\alpha}$ ,  $\Gamma(n_q, \ell) \triangleq \min(\ell^{n_q}, (\ell - 1)\delta n_q)$ ,  $\Gamma'(n_q, \ell) \triangleq \min(\ell^{n_q}, (\ell - 1)\delta n_q + 1)$ ,  $\widehat{Y} = Q(hX + N)$ ,  $N \sim \mathcal{N}(0, 1)$ ,  $\mathcal{P}_X(P_T)$  is the set of distributions on  $\{x_1, x_2, \dots, x_\gamma\}$  such that  $\mathbb{E}(X^2) \leq P_T$ , and  $Q(y) = k$  if  $y \in [t_k, t_{k+1}]$ ,  $k \in \{1, \dots, \gamma-1\}$  and  $Q(y) = 0$  if  $y > t_{\gamma-1}$  or  $y < t_1$ .

We make the following observations regarding the achievable regions in Theorems 3 and 4:

- 1) It can be noted from Equations (4) and (7) that the capacity expression for odd and even values of  $\delta$  are not the same. This is due to Property 6) in Proposition 7 which gives different number of unique codewords for odd and even  $\delta$ . The reason is that while even degree polynomials yield the same output sign as their input converges to  $-\infty$  and  $\infty$ , for odd degree polynomials the output signs are different as their input converges to  $-\infty$  and  $\infty$ . This can potentially yield a larger number of unique codewords in the associated code of the quantizer since the first and last codeword are not equal to each other. This is in contrast with Theorem 3, where the capacity expression is the same for even and odd values of  $\delta$ . The reason is that the for absolute values the output sign is positive as their input converges to  $-\infty$  and  $\infty$ .
- 2) The region given in Theorem 4 strictly contains that of

Theorem 3 for the same value of  $\gamma$ . The reason is that envelope detectors generate absolute value functions which force a symmetric structure on the Voronoi regions of  $Q(\cdot)$ . This manifests in the fully-symmetric condition  $\mathbf{t} \in \mathcal{T}_\gamma$  in Theorem 3 and the properties given in Proposition 3; whereas for polynomial functions, no such symmetry is required and hence the optimization in Theorem 4 is over all  $\mathbf{t} \in \mathbb{R}^\gamma$ . However, as shown in Section VIII generating polynomial operators of degree up to  $\delta$  requires a larger power budget compared to concatenating  $\delta$  envelope detectors. This points to a rate-power tradeoff in using envelope detectors and polynomial operators.

3) One potential approach to improve upon the capacity of the system in Theorem 3 is to augment the envelope detectors by linearly combining their output with the original signal. That is, to generate operators of the form  $f(y) = |y-a|+by$ ,  $a, b \in \mathbb{R}$  instead of  $f(y) = |y-a|$ ,  $a \in \mathbb{R}$ . This removes the fully-symmetric condition  $\mathbf{t} \in \mathcal{T}_\gamma$  in Theorem 3 and yields a larger channel capacity. However, such linear combinations are challenging to implement using analog circuits due to timing issues in synchronizing the output of the envelope detector with the original signal. We hope to address these implementation challenges in future works.

4) For envelope detectors, the dimension  $\gamma$  is equal to  $n_q(\ell - 1)2^\delta$ , whereas for polynomial operators, it is equal to  $n_q(\ell-1)\delta$ . So, the dimension of the optimization space increases faster when concatenating envelope detectors compared to when increasing the polynomial degree. That is, at high SNRs, the capacity in Theorem 3 is larger than that of Theorem 4 for the same value of  $\delta > 1$ . This is also observed in the numerical evaluations in Section VII.

## VI. A HYBRID BEAMFORMING ARCHITECTURE WITH ONE-BIT ADCs

In the previous sections, we have investigated the channel capacity for SISO systems (under analog beamforming) equipped with different collections of implementable analog functions. In this section, we consider hybrid beamforming with one-bit ADCs, where the beamforming vector at the receiver  $\mathbf{w} \in \mathbb{R}^{n_r \times n_s}$  maps the received signal  $Y^{nr}$  to  $\tilde{Y}^{n_s}$ , where  $n_s > 1$  (Figure 2). In this case, we provide a quantization setup, using envelope detectors, which accommodates QAM modulation, and derive an inner bounds to the system capacity. In the next section, we numerically evaluate the resulting capacity and provide comparisons with prior works.

### A. Quantizer Construction

We assume that  $n_q > n_s$ , otherwise, one can use analog beamformers to further reduce the dimension of the beamformer output without performance loss in terms of achievable rates. As mentioned in Section II-A a quantizer is characterized by its analog processing functions  $f_j(\cdot)$ ,  $j \in [n_q]$  and one-bit ADC thresholds  $t^{n_q} \in \mathbb{R}^{n_q}$ . Let us fix a threshold step parameter  $\zeta > 0$ . We take the analog processing functions as follows:

$$f_j(\tilde{Y}^{n_s}) = \begin{cases} \tilde{y}_j & \text{if } j \leq n_s, \\ |\tilde{y}_j| & \text{if } j > n_s, \end{cases}$$

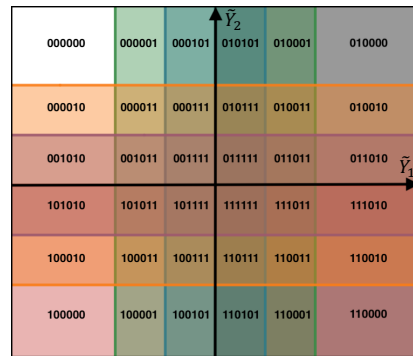


Fig. 7. The quantizer outputs and Voronoi regions in Example 5.

where  $\bar{j}$  is the module  $n_s$  residual of  $j$ . We take the threshold values as follows:

$$t_j = \begin{cases} 0 & \text{if } j \leq n_s, \\ \lfloor \frac{j}{n_q} \rfloor \zeta & \text{if } j > n_s. \end{cases}$$

This choice is clarified through the following example.

**Example 5 (Choice of Thresholds).** Let  $n_s = 2$ ,  $n_q = 6$ , and  $\zeta = 1$ . Then, for the construction described above, the six one-bit ADC operations are as follows:

$$Q_1 : \tilde{y}_1 \leq 0, \quad Q_2 : \tilde{y}_2 \leq 0, \quad Q_3 : |\tilde{y}_1| \leq 1, \\ Q_4 : |\tilde{y}_2| \leq 1, \quad Q_5 : |\tilde{y}_1| \leq 2, \quad Q_6 : |\tilde{y}_2| \leq 2.$$

The quantizer outputs are shown in Figure 7. Note that this resembles a 16-QAM modulation.

### B. Achievable Rates at High SNR

As argued in Section IV, the high SNR capacity is equal to the maximum number of quantization regions which can be generated given the number of ADCs  $n_q$ , with ADC resolution equal to  $\ell$ , and set of implementable analog functions  $\mathcal{F}_a$ . The following theorem provides upper and lower bounds on the high SNR channel capacity of beamforming architectures equipped with envelope detectors for analog signal processing.

**Theorem 5 (High SNR Capacity of Hybrid-Beamforming System).** Assume that the channel matrix observed after beamforming is full-rank, i.e. the rank of  $\mathbf{w}^H \mathbf{h} \mathbf{f}$  is equal to  $n_s$ . Let  $C_{env}(P_T, P_{ADC}, n_s, \delta, \ell)$  denote the channel capacity under power constrain  $P_T$ . Then,

$$n_s \left( 1 + \log(\ell - 1) + \log\left(\frac{n_q - n_s}{n_s}\right) \right) \leq \lim_{P_T \rightarrow \infty} C_{env}(P_T, P_{ADC}, n_s, 1) \leq \log \sum_{k=0}^{n_s} \binom{2(\ell - 1)n_q}{k} \quad (8)$$

where  $n_q = \frac{P_{ADC}}{2\alpha}$ .

The lower bound in Equation (8) is achieved by the quantizer described in this section. To see this, note that by construction, the quantizer partitions each axis into  $2(\ell - 1) \binom{n_q - n_s}{n_s}$  intervals, and each resulting quantization region is mapped to a unique quantizer output (e.g., Figure 7). So, the total number of unique quantizer outputs is  $|C| = (2(\ell - 1) \binom{n_q - n_s}{n_s})^{n_s}$ . The result follows by noting that the communication rate is  $\log |C|$ . The upper bound follows by counting the number of partition

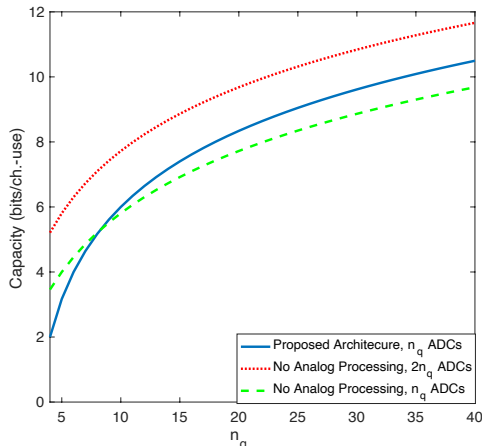


Fig. 8. Channel capacity for i) the proposed architecture and  $n_q$  one-bit ADCs (lower-bound in Theorem 5), ii) no analog processing prior to quantization and  $2n_q$  one-bit ADCs (upper-bound in Theorem 5) and iii) no analog processing prior to quantization and  $n_q$  one-bit ADCs ([30]).

regions generated by  $2(\ell-1)n_q$  hyperplanes in general position in the  $n_s$ -dimensional Euclidean space (e.g. [30]). Figure 8 provides numerical simulations of the i) upper bounds and ii) lower bounds in Equation (8) and iii) the high SNR channel capacity under hybrid beamforming without analog processing derived in [30] for  $n_s = 3$ . It can be observed that the proposed architecture outperforms the one in [30] if the number of one-bit ADCs is larger than  $n_q = 8$ .

## VII. NUMERICAL ANALYSIS OF CHANNEL CAPACITY

In this section, we provide a numerical analysis of the capacity bounds derived in the prequel and evaluate the gains due to the use of nonlinear analog components in the receiver terminal.

### A. Capacity Evaluation for Envelope Detector Architectures

We compute an inner-bound to the capacity expression of the SISO system in Theorem 3, for various SNR values and as a function of the number of ADCs  $n_q$  and the number of concatenated envelope detectors  $\delta$ . To this end, we first use the extension of the Blahut-Arimoto algorithm to discrete memoryless channels with input cost constraints given in [52] to find the best input distribution. Then, we conduct a brute-force search over all possible uniform quantizers. In order to find the mass points of  $X$ , we discretize the real-line using a grid with step-size 0.1, and optimize the distribution over the resulting discrete space. Fig. 9 shows the resulting achievable rates for SNRs in the range of -5 to 40 dB for various values of  $(n_q, \delta)$ . Observe that without nonlinear analog processing, for  $\ell = 2$ , the high SNR capacity is  $\log n_q + 1$  [30]. So, for instance, for  $n_q = \delta = 2$ , the inner bound in Figure 9 surpasses the high SNR capacity without nonlinear analog processing for SNRs higher than 15dB, and its high SNR capacity is more than 25% greater than the case when there is no nonlinear analog processing.

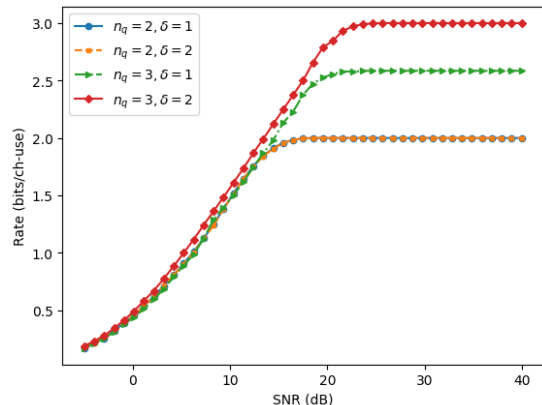


Fig. 9. The set of achievable rates for various values of  $(n_q, \ell, \delta)$  for architectures using envelope detectors.

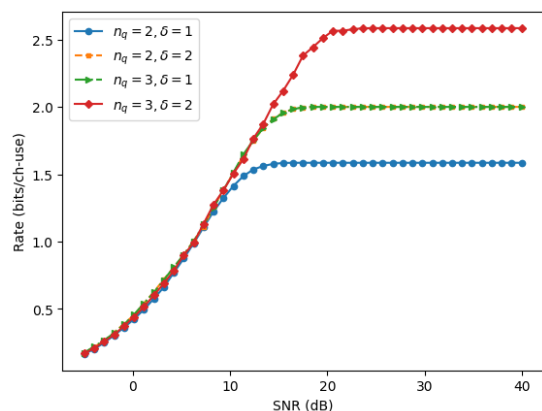


Fig. 10. The set of achievable rates for various values of  $(n_q, \ell, \delta)$  for architectures using polynomial operators.

### B. Capacity Evaluation for Polynomial Operator Architectures

We numerically evaluate the inner bound to the capacity region given in Theorem 4. Similar to the previous case, we first use the extension of the Blahut-Arimoto algorithm to find the best input distribution. Then, we conduct a brute-force search over all possible threshold vectors. To find the mass points of  $X$ , we discretize the real-line using a grid with step-size 0.1, and optimize the distribution over the resulting discrete space. Figure 10 shows the resulting achievable rates for SNRs in the range of -5 to 40 dB for various values of  $(n_q, \delta)$ . It can be observed that the performance improvements due to the use of higher degree polynomials are more significant at high SNRs. Furthermore, it can be observed that the set of achievable rates only depends on  $\min(\ell^{n_q}, (\ell-1)\delta n_q + 1)$ . As a result, for instance the achievable rate when  $n_q = 2, \ell = 2, \delta = 2$  is the same as that of  $n_q = 3, \ell = 2, \delta = 1$  as shown in the figure. So, in this case, using higher degree polynomials can compensate for a lower number of ADCs. On the other hand, the achievable rate for  $n_q = 3, \ell = 2, \delta = 1$  is lower than that of  $n_q = 3, \ell = 2, \delta = 2$  as shown in the figure. So, using higher degree polynomials leads to rate improvements in this scenario.

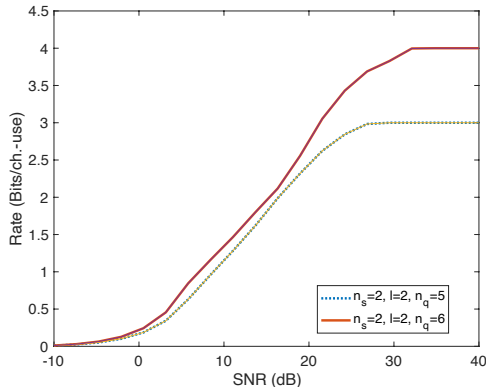


Fig. 11. Inner-bound to achievable rates for the hybrid beamforming architecture of Section VI.

### C. Achievable Inner-Bound for Hybrid Beamforming with Envelope Detectors

We numerically evaluate the inner-bound to the channel capacity which is achievable using the beamforming architecture described in Section VI. We have simulated the communication system for  $n_s = 2$ ,  $\ell = 2$ , and  $n_q \in \{5, 6\}$  and found an estimate of the achievable rates empirically. The results are shown in Figure 11. To perform the simulation, we have optimized the threshold parameter  $\zeta$ , the input alphabet values  $\mathbf{x} \in \mathbb{R}^2$ , and the probability distribution  $P_X$  on the alphabet of the input points using a gradient descent optimization method. We have simulated the channel by generating 15000 independent and identically distributed samples of noise vectors and input messages. We have used the empirical observations to estimate transition probability of the discrete channel resulting from the quantization process. We have used the Blahut-Arimoto algorithm to find the capacity of the resulting channel. It can be observed in Figure 11 that for  $n_q = 5$ , the high SNR rate is larger than the  $n_s \left(1 + \log \left(\frac{n_q - n_s}{n_s}\right)\right)$  lower-bound given in Theorem 4, whereas it is equal to this lower-bound for  $n_q = 6$ .

## VIII. CIRCUIT DESIGN FOR POLYNOMIAL OPERATORS AND ENVELOPE DETECTORS

In this section, we provide power simulation and measurement results using 22 nm FD SOI CMOS technology and 65nm Bulk CMOS technology. These measurements build upon [55]. Figure 12 shows the architecture of a conventional hybrid beamforming receiver (left) and the proposed receiver (right). It can be noted that the main difference between the two architectures is that the linear analog combiner, implemented in baseband, is replaced by a set of non-linear analog operators.

### A. Analysis Based on 65 nm Bulk CMOS Technology

In the following, we provide two circuit designs for envelop detectors and polynomial operators to show the feasibility of the proposed architecture using the 65 nm Bulk CMOS Technology. There are two main advantages to this technology compared to the 22nm technology considered in the sequel: 1) 65 nm technology has a higher nominal supply voltage than 22 nm and if the realized analog operators remain power-efficient,

deploying the proposed receiver architecture across a larger group of CMOS technologies is justified. 2) SOI technologies exhibit more threshold voltage variation compared to the bulk CMOS technologies which will impact the operation of baseband circuitry [56]. Meanwhile, the 22 nm technology offers faster transistors which are better choices for the mm-wave signal chain. Therefore, both single-die designs where baseband and mm-wave chain co-exist on the same chip as well as two-die solutions deploying Bulk CMOS for baseband and SOI CMOS for the mm-wave chain can be pursued.

### B. Polynomial Function Circuit Design

We assume that we are given a direct current (DC) signal (proportional to the bit value) and our objective is to produce a polynomial function of degree up to four of the input DC value. In practice, there are two methods to achieve this objective: (i) DC domain nonlinear function synthesis based on the quadratic I-V characteristic of the transistor and increasing the order of polynomial by cascading circuits [57], (ii) translating DC values to sinusoidal waveforms, and then generating harmonics of these waveforms whose amplitude is polynomially dependent on the fundamental frequency amplitude. The former has a simpler circuitry; however it can only be used to produce a specific set of polynomials, i.e., restricted polynomial coefficient values. The latter can produce polynomials with arbitrary coefficients through efficient filtering of undesired harmonic terms. However, it comes with higher power consumption and more complex circuitry, and its implementation requires careful characterization of transistors' nonlinearity, e.g., using Volterra-Weiner series representation methods [58], [59].

To explain the proposed construction, let us consider the problem of producing the fourth order polynomial  $f(x) = x^4 + x^2$ , where  $x$  is the DC input value. Since naturally the amplitude level of the fourth harmonic is less than that of the second harmonic, for a sinusoidal waveform, a harmonic-centric power enhancement at the fourth harmonic is needed to produce the desired polynomial. Fig. 14(a) shows a circuit to generate  $f(x) = x^4 + x^2$ . In order to generate equal amplitudes at the second and fourth harmonics, the power gain of the transistors generating the fourth harmonic should be larger, leading to an increased power consumption in generating the fourth order term compared to the second order term. Figure 14(b) illustrates numerical values for the power consumption of the proposed circuit through simulations. It can be observed that the ratio of the power consumption for the generation of fourth order term compared to the second order term increases with frequency since the transistor power gain drops at higher frequencies. It is noteworthy that by increasing the baseband bandwidth to support higher data rates, a higher frequency for the generation of polynomials in Fig. 14 may be needed. The simulated results in Fig. 14 are based on 65nm Bulk CMOS technology. The power consumption can be reduced by transitioning into smaller transistor nodes.

### C. Implementation of Envelope Detectors

The circuit block diagram of the proposed multi-step envelope detector is shown in Fig. 15(a). Compared with the

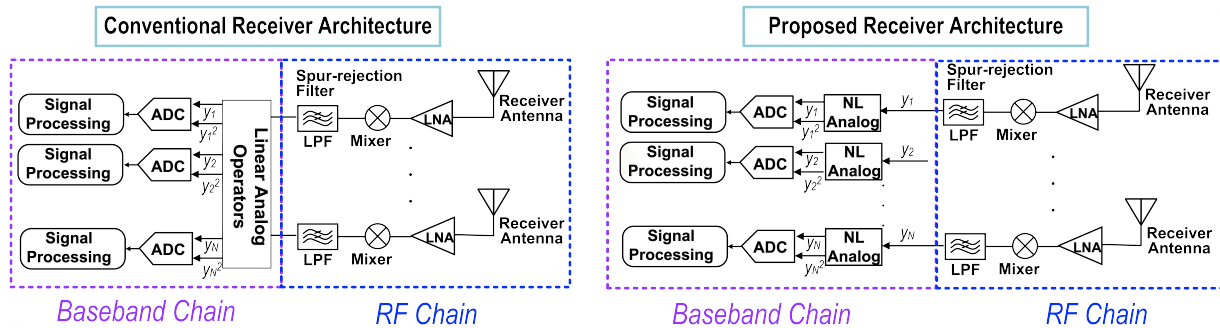


Fig. 12. The block diagram of a MIMO receiver using (left) conventional architectures and (right) proposed architecture.

### Power Breakdown in Conventional Receiver

BF	LNA	Phase Shifter [53]	Combiner <sup>†</sup>	Mixer*	ADC [54] <sup>‡</sup>	Total (mW)	Rate	Rate/Power
Analog	16 × 10	16 × 11.5	1 × 19.5	1 × 14.2	1 × 2 × 70fJ × 2 <sup>8</sup> × 10 <sup>9</sup> × 10 <sup>3</sup>	413.54	8	0.0193
Hybrid (K = 2)	16 × 10	16 × 11.5	2 × 19.5	2 × 14.2	2 × 2 × 70fJ × 2 <sup>8</sup> × 10 <sup>9</sup> × 10 <sup>3</sup>	483.08	16	0.0331

### Power Breakdown in Proposed Receiver (envelope detectors)

BF	LNA	Phase Shifter [53]	Combiner <sup>†</sup>	Mixer*	NL Operator	ADC [54] <sup>‡</sup>	Total (mW)	Rate	Rate/Power
Analog	16 × 10	16 × 11.5	1 × 19.5	1 × 14.2	1 × 3	32 × 2 × 70fJ × 2 <sup>3</sup> × 10 <sup>9</sup> × 10 <sup>3</sup>	416.54	8.807	0.0211
Hybrid (K = 2)	16 × 10	16 × 11.5	2 × 19.5	2 × 14.2	2 × 3	64 × 2 × 70fJ × 2 <sup>3</sup> × 10 <sup>9</sup> × 10 <sup>3</sup>	489.08	17.615	0.0360

### Power Breakdown in Proposed Receiver (2nd order polynomial)

BF	LNA	Phase Shifter [53]	Combiner <sup>†</sup>	Mixer*	NL Operator	ADC [54] <sup>‡</sup>	Total (mW)	Rate	Rate/Power
Analog	16 × 10	16 × 11.5	1 × 19.5	1 × 14.2	1 × 5	32 × 2 × 70fJ × 2 <sup>3</sup> × 10 <sup>9</sup> × 10 <sup>3</sup>	418.54	8.807	0.0210
Hybrid (K = 2)	16 × 10	16 × 11.5	2 × 19.5	2 × 14.2	2 × 5	64 × 2 × 70fJ × 2 <sup>3</sup> × 10 <sup>9</sup> × 10 <sup>3</sup>	493.08	17.615	0.0357

### Power Breakdown in Proposed Receiver (4th order polynomial)

BF	LNA	Phase Shifter [53]	Combiner <sup>†</sup>	Mixer*	NL Operator	ADC [54] <sup>‡</sup>	Total (mW)	Rate	Rate/Power
Analog	16 × 10	16 × 11.5	1 × 19.5	1 × 14.2	1 × 10	32 × 2 × 70fJ × 2 <sup>3</sup> × 10 <sup>9</sup> × 10 <sup>3</sup>	423.54	9.807	0.0232
Hybrid (K = 2)	16 × 10	16 × 11.5	2 × 19.5	2 × 14.2	2 × 10	64 × 2 × 70fJ × 2 <sup>3</sup> × 10 <sup>9</sup> × 10 <sup>3</sup>	503.08	19.615	0.0390

<sup>†</sup> For each RX, a four bit binary weighted current adder is implemented with 1.6mW power consumption

<sup>‡</sup> Both power consumption of one-bit-ADC and 8-bit-ADC are normalized from the reference

<sup>‡</sup> For the 4th order polynomial, the data rate and subsequently the count of ADCs is twice that of second order polynomial.

Fig. 13. The breakdown of power consumption for the receiver in a conventional architecture and the proposed architecture. It is evident that the proposed architecture lowers the total power consumption of the entire receiver chain substantially

conventional pipe-line ADC shown in Fig. 15(b) this circuit exhibits major power saving by removing the one-bit DAC and subtractor used in each stage. In terms of functionality, the linearity in both scenarios is mainly limited by gain and bandwidth of operational amplifiers (Op-amp) used in functional blocks.

The operational amplifiers deployed in the envelope detector are two-stage differential to single-ended amplifiers with gain-bandwidth product (GBW) of 32 GHz in Fig. 16(a). This GBW allows to amplify signals up to 10 GHz with a gain above 15 dB, which is critical for the operation of the envelope detector shown in Fig. 16(b). The resistors in this circuit establish a trade-off between the bandwidth and the waveform distortion. In other words, the larger resistance value leads to smaller distortion of the flipping negative part at the expense of increasing the resistance associated with the output pole of each envelope detector stage, and subsequently limiting the bandwidth of operation. In our simulations, we assumed 500Ω resistors. According to the simulation results shown in Fig. 17, the higher gain of each operational amplifier leads to smaller amplitude distortion at the output, which naturally is achieved at the expense of a smaller bandwidth for the amplifier, thereby leading to a distortion-bandwidth tradeoff.

By cascading multiple stages of the envelope detectors, as

mentioned in Section IV the achievable data-rate increases. To justify this claim, we have simulated the two-stage envelope detector circuit in Fig. 15(a). The DC level shifter is realized by diode-based circuits which consume no DC power and can operate up to 6 GHz.

The simulated eye-diagram performance of the two-stage envelope detector is illustrated in Fig. 18. It can be noted that at such higher data rates (12 Gb/s), in contrast to lower data rates where a square wave is feasible, sinusoidal waveforms are the only feasible inputs to an ADC [60]. Therefore, in our simulations we consider the input to the absolute value function circuitry to be a sinusoidal waveform due to the slewing effects [61].

An important characteristic of the envelope detectors is the input dynamic range to support an output waveform that follows the input amplitude with minimal deviation. By increasing the input magnitude, the amplifier's constituent transistors will be pushed into nonlinear regions of operation, and a "compression behavior" is observed. The point at which this compression happens is an upper-bound on the magnitude of input signals. This value is critical in scenarios where amplitude modulation is deployed in the transceiver. To evaluate our proposed envelope detector, two modulation scenarios of Pulse Amplitude Modulation (PAM)4 and PAM8 modulation

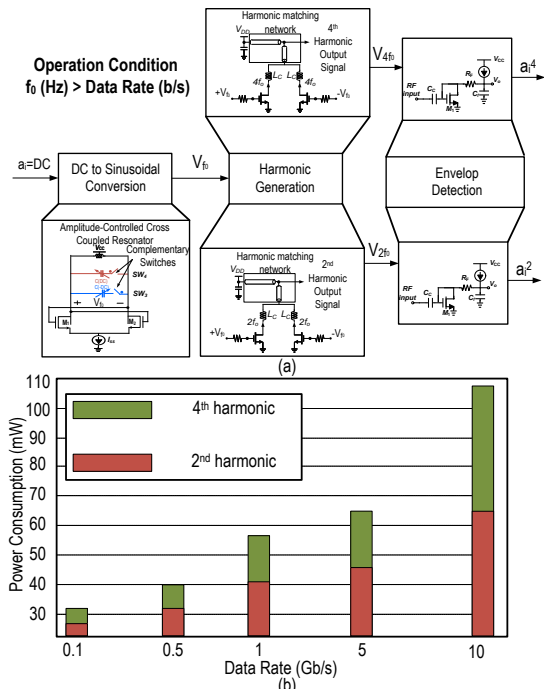


Fig. 14. (a) The circuit design for the generation of fourth and second order polynomials, (b) the power consumption breakdown of the circuits for generation of equal voltage amplitude (corresponding to 0 dBm power) at the second and fourth harmonics.

schemes are considered as the input to the envelope detector, as shown in Fig. 18. In both cases, the output rectified eye diagram exhibits clear distinction between the amplitude levels (denoted by different colors) such that the comparators in the following one-bit ADCs can distinguish the amplitude levels with small error. The simulation results in Fig. 18 demonstrate that the amplitude ratios at the output follow the input amplitude ratios even when the dynamic range of input waveform is only between -400 to +400 mV. I can be noted that a PAM-8 waveform in the receiver base-band can be constructed by passing the QAM-64 signal (in Table I) through a quadrature down-conversion mixer [62].

Theorems 2 and 4 show that the channel capacity depends on the number of ADCs through  $n_q 2^{\delta_{env}} + 1$  and  $n_q \delta_{poly} + 1$ , respectively, so that the use of an envelope detector and quadratic analog operators instead of a linear operator ( $\delta_{env} : 0 \rightarrow 1$  and  $\delta_{poly} : 1 \rightarrow 2$ ) has an equivalent effect on capacity as that of quadrupling and doubling the number of ADCs  $n_q$ , respectively. This fact, along with the power consumption values given in Figures 13 and 19 justify the use of nonlinear analog operators. It is understood that power consumption is dependent on circuit configuration, transistor size, and passive quality factors. However, the values reported in this paper based on recent demonstrations of a mm-wave transceiver in a 22 nm FDSOI CMOS technology serve as a proof-of-concept to justify the effectiveness of the proposed receiver architecture designs.

#### D. Analysis Based on 22 nm FDSOI CMOS Technology

In the Figure 13, the itemized and total power consumption is compared between the two architectures in a 22 nm FDSOI CMOS technology. For the power values in Fig-

13, we assume a mm-wave carrier frequency of 60 GHz, RF bandwidth of 1 GHz, and 16 channels. The reported power consumption for RF elements are based on the measurement results of the chip reported in [55] and the power consumption of nonlinear operators and ADCs are based on post-layout simulation results and analytical values in [63], respectively.

## IX. CONCLUSION

The application of nonlinear analog operations in MIMO receivers was considered. A receiver architecture consisting of linear analog combiners, implementable nonlinear analog operators, and few-bit threshold ADCs was designed, and the fundamental information theoretic performance limits of the resulting communication system were investigated. Furthermore, circuit-level simulations, using a 22 nm FDSOI CMOS technology, were provided to show the implementability of the desired nonlinear analog operators with practical power budgets.

## APPENDIX A

### PROOF OF PROPOSITION 1

Let  $n_q = \lfloor \frac{P_{ADC}}{2\sigma} \rfloor$ . For a given quantizer with associated code  $C$ , the high SNR achievable rate is  $\log |P| = \log |C|$ . So, finding the capacity is equivalent to finding the maximum  $|C|$  over all choices of  $Q(\cdot)$ . First, let us prove the converse result. Note that  $|C| \leq 2n_q$  since  $\mathbf{c}_0 = \mathbf{c}_{2n_q}$ . The reason is that for the absolute value function  $f_{a,j}(\cdot)$ ,  $j \in [n_q]$ , we have  $\lim_{y \rightarrow \infty} f_{a,j}(y) = \lim_{y \rightarrow -\infty} f_{a,j}(y) = \infty$ . So,

$$c_{0,j} = \lim_{y \rightarrow -\infty} \mathbb{1}(f_{a,j} - t_j > 0) = \lim_{y \rightarrow \infty} \mathbb{1}(f_{a,j} - t_j > 0) = c_{2n_q,j}. \quad (9)$$

As a result,  $\log |C| \leq 1 + \log n_q$ . Next, we prove achievability. Let  $t_j = \frac{n_q+1}{2}$ ,  $j \in [n_q]$  and  $f_{a,j}(y) \triangleq |y - j - \frac{n_q+1}{2}|$ ,  $j \in [n_q]$ , so that the roots of  $f_{a,j}(\cdot) - t_j$  are  $j$  and  $j - n_q - 1$ . Then,  $(r_1, r_2, \dots, r_{2n_q}) = (-n_q, -n_q+1, \dots, -1, 1, 2, \dots, n_q)$  and

$$c(i, j) = \begin{cases} 1 - \mathbb{1}(j \leq i) & \text{if } i \leq n_q, \\ \mathbb{1}(n_q - j + 1 \leq i - n_q) & \text{otherwise.} \end{cases}$$

For instance, for  $n_q = 3$ , we have  $C = (111, 011, 001, 000, 001, 011, 111)$ . Hence, the only repeated codewords are  $\mathbf{c}_0$  and  $\mathbf{c}_{2n_q}$ . As a result,  $|C| = 2n_q$ , and  $\log |C| = 1 + \log n_q$  is achievable.  $\square$

## APPENDIX B

### PROOF OF THEOREM 1

We provide an outline of the proof. Note that the input alphabet has at most  $2n_q + 1$  mass points since based on the proof of Proposition 1, the channel output can take at most  $2n_q$  values. Let the quantized channel output be denoted by  $\hat{Y}$ . Since the conditional measure  $P_{\hat{Y}|X}(\cdot|x)$ ,  $x \in \mathbb{R}$  is continuous in  $x$ , and  $\lim_{x \rightarrow \infty} P_{\hat{Y}|X}(\mathcal{A}|x) = \mathbb{1}(\hat{y} \in \mathcal{A})$ ,  $\mathcal{A} \in \mathbb{B}$  for some fixed  $\hat{y}$ , the conditions in the proof of [64, Prop. 1] hold, and the optimal input distribution has bounded support. From the extension of Witsenhausen's result [65] given in [64, Prop. 2], the optimal input distribution is discrete and takes at most  $2n_q + 1$  values. This completes the proof of converse. To prove

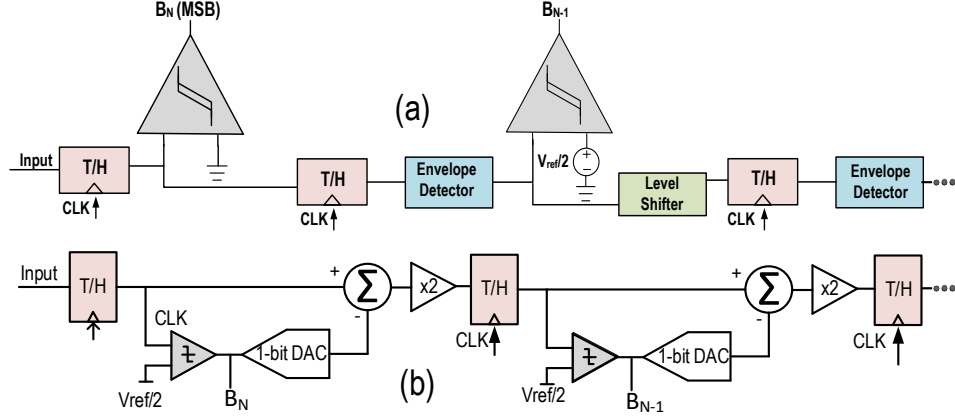


Fig. 15. (a) The cascade of circuits emulating absolute value operators, (b) conventional pipeline ADC architecture.

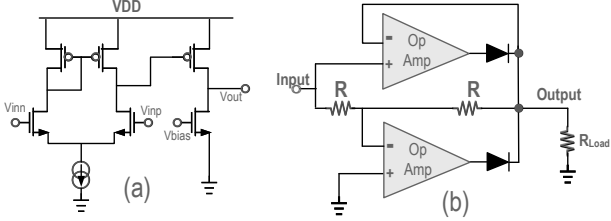


Fig. 16. (a) The deployed differential to single-ended op-amp deployed in the envelope detector (b) the circuit diagram of the implemented envelope detector

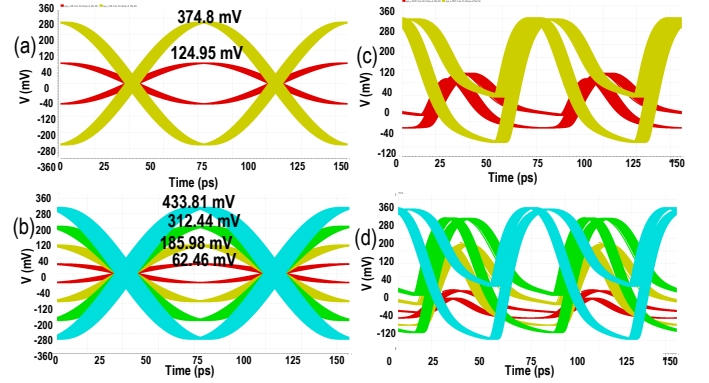


Fig. 18. The input waveform eye diagram for (a) PAM4 and (b) PAM8 modulations compared with the corresponding envelope detector output eye diagrams in (c) and (d).

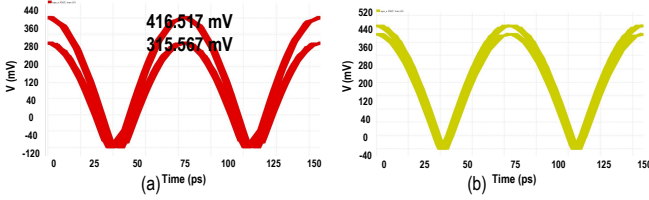


Fig. 17. The impact of amplifier gain on the half-cycle rectification amplitude distortion illustrated for (a) gain of 10 dB, and (b) 25 dB.

achievability, it suffices to show that one can choose the set of functions  $f_{a,j}(\cdot)$ ,  $j \in [n_q]$  and quantization thresholds  $t_j$ ,  $j \in [n_q]$  such that the resulting quantizer operates as described in the theorem statement, i.e., it generates  $\tilde{Y} = Q(hX + N)$  where  $Q(y) = k$  if  $y \in [t_k, t_{k+1}]$ ,  $k \in \{1, \dots, 2n_q\}$  and  $Q(y) = 0$  if  $y > t_{2n_q}$  or  $y < t_1$ . To this end, let  $\mathbf{t}^*$  be the optimal quantizer thresholds in (2). Let  $r_1, r_2, \dots, r_{2n_q}$  be the elements of  $\mathbf{t}^*$  written in non-decreasing order. Define a quantizer with associated analog functions  $f_{a,j}(y) \triangleq |y - \frac{r_j + r_{n_q+j}}{2}|$  and  $t_j = \frac{r_{n_q+j} - r_j}{2}$ . Note that  $t_j > 0$  since  $r_j, j \in [n_q]$  are non-decreasing. Then, similar to the proof of Proposition 1, the quantization rule gives distinct outputs for  $y \in [r_k, r_{k+1}]$ ,  $k \in \{1, \dots, 2n_q\}$  and  $y \in [r_{2n_q}, \infty) \cup [-\infty, r_1]$  as desired.  $\square$

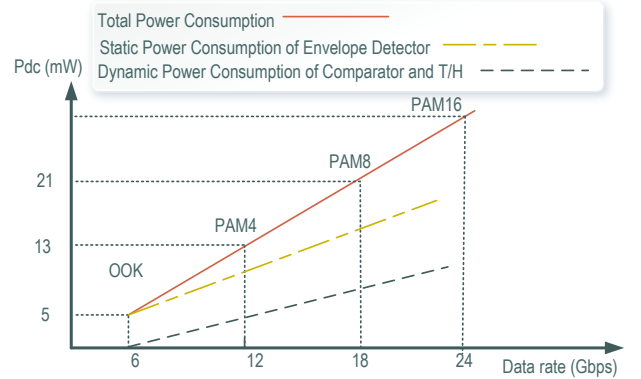


Fig. 19. The linear growth of power consumption with the data rate in the nonlinear analog operator circuits, i.e., the polynomial generators and envelope detectors.

## APPENDIX C PROOF OF PROPOSITION 5

For  $j \in [n_q]$  and non-decreasing vector  $(r_{i_1}, r_{i_2}, \dots, r_{i_{2^\delta}})$  where  $i_\lambda \in \mathcal{I}_j$ ,  $j \in [n_q]$ ,  $\lambda \in [2^\delta]$ , define

$$a_{1,j} \triangleq \frac{r_{i_1} + r_{i_{2^\delta}}}{2}, \quad a_{s,j} \triangleq \frac{r_{i_{2^\delta}} + r_{i_{2^s}}}{2} - \sum_{s'=1}^{s-1} a_{s',j}, \quad 1 < s \leq \delta,$$

$$t_j \triangleq r_{i_{2^\delta}} - \sum_{s=1}^{\delta-1} a_{s',j}, \quad 1 < s \leq \delta$$

where  $\eta_s \triangleq 2^\delta - \sum_{s'=1}^{s-1} 2^{\delta-s'} + 1$ ,  $s > 1$ . Consider a quantizer  $Q(\cdot)$  with ADC thresholds  $t(1 : n_q)$  and associated analog functions  $f_j(y) \triangleq A_\delta(x, a^\delta)$ ,  $j \in [n_q]$ . Then,  $r_1, r_2, \dots, r_\gamma$  are the non-decreasing sequence of roots of  $f_j(\cdot)$ ,  $j \in [n_q]$ , and the associated code of the quantizer  $Q(\cdot)$  is  $C$  as desired.  $\square$

#### APPENDIX D PROOF OF PROPOSITION 6

We provide an outline of the proof. Let us consider the following cases:

**Case 1:**  $\sum_{j=1}^{n_q} \kappa_j \geq 2^{n_q}$

In this case, one can use a balanced Gray code [50] to construct  $C$ . A balanced Gray code is a (binary) code where consecutive codewords have Hamming distance equal to one, and each of the bit positions changes value either  $2\lfloor \frac{2^{n_q}}{2n_q} \rfloor$  times or  $2\lceil \frac{2^{n_q}}{2n_q} \rceil$  times. If  $\min_{j \in [n_q]} \kappa_j \geq 2\lceil \frac{2^{n_q}}{2n_q} \rceil$  the proof is complete as one can concatenate the balanced gray code with a series of additional repeated codewords to satisfy the transition counts, and since the balanced gray code is a subcode of the resulting code, we have  $|C| = 2^{n_q}$ . Otherwise, there exists  $j \in [n_q]$  such that  $\kappa_j < 2\lceil \frac{2^{n_q}}{2n_q} \rceil$ . In this case, without loss of generality, let us assume that  $\kappa_1 \leq \kappa_2, \dots \leq \kappa_{n_q}$ . Note that since  $|\kappa_j - \kappa_{j'}| \leq 2$ ,  $j, j' \in [n_q]$  and  $\kappa_j, j \in [n_q]$  are even, there is at most one  $j^* \in [n_q]$  such that  $\kappa_{j^*} \leq \kappa_{j^*+1}$ . Let  $\kappa'_1, \kappa'_2, \dots, \kappa'_{n_q}$  be the transition count sequence of a balanced gray code  $C'$  written in non-decreasing order. Note that  $2\lceil \frac{2^{n_q}}{2n_q} \rceil - 2\lfloor \frac{2^{n_q}}{2n_q} \rfloor = 2$ . Hence, similar to the above argument, there can only be one  $j' \in [n_q]$  for which  $\kappa_{j'} \leq \kappa_{j'+1}$ . Since  $\sum_{j=1}^{n_q} \kappa_j \geq 2^{n_q} = \sum_{j=1}^{n_q} \kappa'_j$ , we must have  $j^* \leq j'$ . So, the balanced gray code can be used as a subcode similar to the previous case by correctly ordering the bit positions to match the order of  $\kappa_j, j \in [n_q]$ . This completes the proof.

**Case 2:**  $\sum_{j=1}^{n_q} \kappa_j < 2^{n_q}$

The proof is based on techniques used in the construction of balanced Gray codes [50]. We prove the result by induction on  $n_q$ . The proof for  $n_q = 1, 2$  is straightforward and follows by construction of length-one and length-two sequences. For  $n_q > 2$ , Assume that the result holds for all  $n'_q \leq n_q$ . Without loss of generality, assume that  $\kappa_1 \leq \kappa_2, \dots \leq \kappa_{n_q}$ . The proof considers four sub-cases as follows.

**Case 2.i:**  $\sum_{j=3}^{n_q} \kappa_j \in [0, 2^{n_q-2}]$

In this case, by the induction assumption, there exists  $C'$ , a code with codewords of length  $n_q - 2$ , whose transition sequence is  $\kappa_3, \kappa_4, \dots, \kappa_{n_q}$ , and  $|C'| = \sum_{j=3}^{n_q} \kappa_j$ . We construct  $C$  from  $C'$  as follows. Let  $\mathbf{c}_0 = (0, 0, \mathbf{c}'_0)$ ,  $\mathbf{c}_1 = (0, 1, \mathbf{c}'_0)$ ,  $\mathbf{c}_2 = (1, 1, \mathbf{c}'_0)$ ,  $\mathbf{c}_3 = (1, 0, \mathbf{c}'_0)$ ,  $\mathbf{c}_4 = (1, 0, \mathbf{c}'_1)$ ,  $\mathbf{c}_5 = (0, 0, \mathbf{c}'_1)$ ,  $\mathbf{c}_6 = (0, 1, \mathbf{c}'_1)$ ,  $\mathbf{c}_7 = (1, 1, \mathbf{c}'_1), \dots$ . This resembles the procedure for constructing balanced gray codes [50]. We continue concatenating the first two bits of each codeword in  $C$  to the codewords in  $C'$  using the procedure described above until  $\kappa_1$  transitions for position 1 and  $\kappa_2$  transitions for position 2 have taken place. Note that this is always possible since i) for each two codewords in  $C'$ , we 'spend' two transitions of each of the first and second positions in  $C$  to produce four new codewords, ii)  $\kappa_2 - \kappa_1 \leq 2$ , and iii)  $\kappa_2 \leq \sum_{j=3}^{n_q} \kappa_j$ , where the latter condition ensures that we do not run out of codewords in  $C'$  before the necessary transitions in positions 1 and 2 are completed.

After  $\kappa_2 + 1$  codewords, the transitions in positions 1 and 2 are completed, and the last produced codeword is  $(0, 0, \mathbf{c}'_{\kappa_2+1})$  since  $\kappa_1$  and  $\kappa_2$  are both even. To complete the code  $C$ , we add  $(0, 0, \mathbf{c}'_i)$ ,  $i \in [\kappa_2 + 2, \sum_{j=3}^{n_q} \kappa_j]$ . Then, by construction, we have  $|C| = |C'| + \kappa_1 + \kappa_2 = \sum_{j=1}^{n_q} \kappa_j$  and the code satisfied Properties 1), 2), 3), and 5) in Proposition 4.

**Case 2.ii:**  $\sum_{j=3}^{n_q} \kappa_j \in [2^{n_q-2}, 2^{n_q-1}]$

Similar to the previous case, let  $C'$  be a balanced gray code with codeword length  $n_q - 2$  and transition counts  $\kappa'_1 \leq \kappa'_2 \leq \dots \leq \kappa'_{n_q-2}$ . Define  $\kappa'_j = \kappa_j - \kappa'_{j+2}$ ,  $j \in \{3, 4, \dots, n_q\}$ . Note that  $\kappa'_j$  satisfy the conditions on transition counts in the proposition statement, and hence by the induction assumption, there exists a code  $C''$  with transition counts  $\kappa''_j$ ,  $j \in [n_q - 2]$ . The proof is completed by appropriately concatenating  $C'$  and  $C''$  to construct  $C$ . Let  $\gamma''$  be the number of codewords in  $C''$  and define  $\mathbf{c}_i = (0, 0, \mathbf{c}''_i)$ ,  $i \in [\gamma'']$ ,  $\mathbf{c}_{\gamma''+1} = (0, 1, \mathbf{c}''_{\gamma''})$ ,  $\mathbf{c}_{\gamma''+2} = (1, 1, \mathbf{c}''_{\gamma''})$ ,  $\mathbf{c}_{\gamma''+3} = (1, 0, \mathbf{c}''_{\gamma''})$ ,  $\mathbf{c}_{\gamma''+4} = (1, 0, \mathbf{c}'_1), \dots$ . Similar to the previous case, it is straightforward to show that this procedure yields a code  $C$  with the desired transition sequence.

The proof for the two subcases where  $\sum_{j=3}^{n_q} \kappa_j \in [2^{n_q-1}, 3 \times 2^{n_q-2}]$  and  $\sum_{j=3}^{n_q} \kappa_j \in [3 \times 2^{n_q-1}, 2^{n_q}]$  is similar and is omitted for brevity.

#### REFERENCES

- [1] Farhad Shirani and Hamidreza Aghasi. Mimo systems with one-bit adcs: Capacity gains using nonlinear analog operations. In *2022 IEEE International Symposium on Information Theory (ISIT)*, pages 2511–2516, 2022.
- [2] Farhad Shirani and Hamidreza Aghasi. Quantifying the capacity gains in coarsely quantized siso systems with nonlinear analog operators. *arXiv preprint arXiv:2208.04450*, 2022.
- [3] Ahmed M Al-samman, Marwan Hadri Azmi, and Tharek Abd Rahman. A survey of millimeter wave (mm-wave) communications for 5g: Channel measurement below and above 6 ghz. In *International Conference of Reliable Information and Communication Technology*, pages 451–463. Springer, 2018.
- [4] Heedong Do, Sungmin Cho, Jeonghun Park, Ho-Jin Song, Namyoon Lee, and Angel Lozano. Terahertz line-of-sight mimo communication: Theory and practical challenges. *IEEE Communications Magazine*, 59(3):104–109, 2021.
- [5] Boris Murmann et al. Adc performance survey 1997-2016, 2018.
- [6] Boris Murmann. The race for the extra decibel: a brief review of current ADC performance trajectories. *IEEE Solid-State Circuits Magazine*, 7(3):58–66, 2015.
- [7] Jiayi Zhang, Linglong Dai, Xu Li, Ying Liu, and Lajos Hanzo. On low-resolution adcs in practical 5g millimeter-wave massive mimo systems. *IEEE Communications Magazine*, 56(7):205–211, 2018.
- [8] Theodore S Rappaport, Robert W Heath Jr, Robert C Daniels, and James N Murdock. *Millimeter wave wireless communications*. Pearson Education, 2015.
- [9] Hadi Sarieeddeen, Mohamed-Slim Alouini, and Tareq Y Al-Naffouri. An overview of signal processing techniques for terahertz communications. *Proceedings of the IEEE*, 2021.
- [10] Christina Chaccour, Mehdi Naderi Soorki, Walid Saad, Mehdi Bennis, Petar Popovski, and M erouane Debbah. Seven defining features of terahertz (thz) wireless systems: A fellowship of communication and sensing. *IEEE Communications Surveys & Tutorials*, 24(2):967–993, 2022.
- [11] Najath Akram, Arjuna Madanayake, Satheesh B Venkatakrishnan, John L Volakis, Dimitra Psychogiou, Thomas L Marzetta, and Theodore S Rappaport. Massive-mimo and digital mm-wave arrays on rf-socs using fdm for m-fold increase in antennas per adc/dac. In *2021 IEEE Space Hardware and Radio Conference (SHARC)*, pages 25–27. IEEE, 2021.



- [12] Robert W Heath, Nuria Gonzalez-Prelcic, Sundeep Rangan, Wonil Roh, and Akbar M Sayeed. An overview of signal processing techniques for millimeter wave MIMO systems. *IEEE journal of selected topics in signal processing*, 10(3):436–453, 2016.
- [13] Roi Méndez-Rial, Cristian Rusu, Ahmed Alkhateeb, Nuria González-Prelcic, and Robert W Heath. Channel estimation and hybrid combining for mmwave: Phase shifters or switches? In *2015 Information Theory and Applications Workshop (ITA)*, pages 90–97. IEEE, 2015.
- [14] Robert H Walden. Analog-to-digital converter survey and analysis. *IEEE Journal on selected areas in communications*, 17(4):539–550, 1999.
- [15] Dan Li, Deli Qiao, and Lei Zhang. Achievable rate of indoor thz communication systems with finite-bit adcs. In *2018 10th International Conference on Wireless Communications and Signal Processing (WCSP)*, pages 1–6. IEEE, 2018.
- [16] Boyu Ning, Zhongbao Tian, Zhi Chen, Chong Han, Jinhong Yuan, and Shaoqian Li. Prospective beamforming technologies for ultra-massive mimo in terahertz communications: A tutorial. *arXiv preprint arXiv:2107.03032*, 2021.
- [17] Chong Han, Longfei Yan, and Jinhong Yuan. Hybrid beamforming for terahertz wireless communications: Challenges, architectures, and open problems. *IEEE Wireless Communications*, 28(4):198–204, 2021.
- [18] Andreas F Molisch, Vishnu V Ratnam, Shengqian Han, Zheda Li, Sinh Le Hong Nguyen, Linsheng Li, and Katsuyuki Haneda. Hybrid beamforming for massive MIMO: A survey. *IEEE Communications Magazine*, 55(9):134–141, 2017.
- [19] Ahmed Alkhateeb, Jianhua Mo, Nuria Gonzalez-Prelcic, and Robert W Heath. MIMO precoding and combining solutions for millimeter-wave systems. *IEEE Communications Magazine*, 52(12):122–131, 2014.
- [20] Abbas Khalili, Shahram Shahsavari, Farhad Shirani, Elza Erkip, and Yonina C Eldar. On throughput of millimeter wave MIMO systems with low resolution ADCs. In *ICASSP 2020-2020 IEEE International Conference on Acoustics, Speech and Signal Processing (ICASSP)*, pages 5255–5259. IEEE, 2020.
- [21] Sourjya Dutta, Abbas Khalili, Elza Erkip, and Sundeep Rangan. Capacity bounds for communication systems with quantization and spectral constraints. In *2020 IEEE International Symposium on Information Theory (ISIT)*, pages 2038–2043. IEEE, 2020.
- [22] Christopher Mollén, Junil Choi, Erik G Larsson, and Robert W Heath. Achievable uplink rates for massive mimo with coarse quantization. In *2017 IEEE International Conference on Acoustics, Speech and Signal Processing (ICASSP)*, pages 6488–6492. IEEE, 2017.
- [23] Christopher Mollen, Junil Choi, Erik G Larsson, and Robert W Heath. One-bit adcs in wideband massive mimo systems with ofdm transmission. In *2016 IEEE International Conference on Acoustics, Speech and Signal Processing (ICASSP)*, pages 3386–3390. IEEE, 2016.
- [24] Sven Jacobsson, Giuseppe Durisi, Mikael Coldrey, Ulf Gustavsson, and Christoph Studer. Throughput analysis of massive mimo uplink with low-resolution adcs. *IEEE Transactions on Wireless Communications*, 16(6):4038–4051, 2017.
- [25] Hessam Pirzadeh and A Lee Swindlehurst. Spectral efficiency of mixed-adc massive mimo. *IEEE Transactions on Signal Processing*, 66(13):3599–3613, 2018.
- [26] Yongzhi Li, Cheng Tao, Gonzalo Seco-Granados, Amine Mezghani, A Lee Swindlehurst, and Liu Liu. Channel estimation and performance analysis of one-bit massive mimo systems. *IEEE Transactions on Signal Processing*, 65(15):4075–4089, 2017.
- [27] Jianhua Mo, Philip Schniter, and Robert W Heath. Channel estimation in broadband millimeter wave MIMO systems with few-bit ADCs. *IEEE Transactions on Signal Processing*, 66(5):1141–1154, 2017.
- [28] Neil Irwin Bernardo, Jingge Zhu, Yonina C. Eldar, and Jamie Evans. Capacity bounds for one-bit mimo gaussian channels with analog combining. *IEEE Transactions on Communications*, 70(11):7224–7239, 2022.
- [29] Timur Zirtiloglu, Nir Shlezinger, Yonina C. Eldar, and Rabia Tugce Yazicigil. Power-efficient hybrid mimo receiver with task-specific beamforming using low-resolution adcs. In *ICASSP 2022 - 2022 IEEE International Conference on Acoustics, Speech and Signal Processing (ICASSP)*, pages 5338–5342, 2022.
- [30] Abbas Khalili, Farhad Shirani, Elza Erkip, and Yonina C Eldar. MIMO networks with one-bit ADCs: Receiver design and communication strategies. *IEEE Transactions on Communications*, 2021.
- [31] R.E. Suarez, P.R. Gray, and D.A. Hodges. All-mos charge-redistribution analog-to-digital conversion techniques. ii. *IEEE Journal of Solid-State Circuits*, 10(6):379–385, 1975.
- [32] Xiyuan Tang, Jiabin Liu, Yi Shen, Shaolan Li, Linxiao Shen, Arindam Sanyal, Kareem Ragab, and Nan Sun. Low-power sar adc design: Overview and survey of state-of-the-art techniques. *IEEE Transactions on Circuits and Systems I: Regular Papers*, 69(6):2249–2262, 2022.
- [33] A. E. Gamal and Y. H. Kim. *Network Information Theory*. Cambridge University Press, 2011.
- [34] Theodore S. Rappaport. *Wireless communications - principles and practice*. Prentice Hall, 1996.
- [35] Behzad Razavi. *Principles of data conversion system design*, volume 126. IEEE press New York, 1995.
- [36] Jianhua Mo and Robert W Heath. High SNR capacity of millimeter wave MIMO systems with one-bit quantization. In *Information Theory and Applications Workshop (ITA)*, 2014, pages 1–5. IEEE, 2014.
- [37] Jianhua Mo and Robert W Heath. Capacity analysis of one-bit quantized MIMO systems with transmitter channel state information. *IEEE transactions on signal processing*, 63(20):5498–5512, 2015.
- [38] Jianhua Mo, Ahmed Alkhateeb, Shadi Abu-Surra, and Robert W Heath. Hybrid architectures with few-bit ADC receivers: Achievable rates and energy-rate tradeoffs. *IEEE Transactions on Wireless Communications*, 16(4):2274–2287, 2017.
- [39] Sven Jacobsson, Giuseppe Durisi, Mikael Coldrey, Ulf Gustavsson, and Christoph Studer. One-bit massive MIMO: Channel estimation and high-order modulations. In *2015 IEEE International Conference on Communication Workshop (ICCW)*, pages 1304–1309. IEEE, 2015.
- [40] Josef A Nossek and Michel T Ivrlac̃. Capacity and coding for quantized MIMO systems. In *Proceedings of the 2006 international conference on Wireless communications and mobile computing*, pages 1387–1392. ACM, 2006.
- [41] Xinying Zhang, Andreas F Molisch, and Sun-Yuan Kung. Variable-phase-shift-based RF-baseband codesign for MIMO antenna selection. *IEEE Transactions on Signal Processing*, 53(11):4091, 2005.
- [42] Pallav Sudarshan, Neelesh B Mehta, Andreas F Molisch, and Jin Zhang. Channel statistics-based RF pre-processing with antenna selection. *IEEE Transactions on Wireless Communications*, 5(12):3501–3511, 2006.
- [43] Tobias Koch and Amos Lapidoth. At low SNR, asymmetric quantizers are better. *IEEE Transactions on Information Theory*, 59(9):5421–5445, 2013.
- [44] Abbas Khalili, Stefano Rini, Luca Barletta, Elza Erkip, and Yonina C Eldar. On MIMO channel capacity with output quantization constraints. In *2018 IEEE International Symposium on Information Theory (ISIT)*, pages 1355–1359. IEEE, 2018.
- [45] Jingbo Tan and Linglong Dai. Thz precoding for 6g: Applications, challenges, solutions, and opportunities. *arXiv preprint arXiv:2005.10752*, 2020.
- [46] Thomas M. Cover. Geometrical and statistical properties of systems of linear inequalities with applications in pattern recognition. *IEEE Trans. Electron. Comput.*, EC-14, no.3:326–334, Jun. 1965.
- [47] Gerald L Alexanderson and John E Wetzel. Simple partitions of space. *Mathematics magazine*, 51(4):220–225, 1978.
- [48] RO Winder. Partitions of n-space by hyperplanes. *SIAM Journal on Applied Mathematics*, 14(4):811–818, 1966.
- [49] Thomas Kleine-Ostmann and Tadao Nagatsuma. A review on terahertz communications research. *Journal of Infrared, Millimeter, and Terahertz Waves*, 32(2):143–171, 2011.
- [50] Girish S Bhat and Carla D Savage. Balanced gray codes. *the electronic journal of combinatorics*, 3(1):R25, 1996.
- [51] Igor Sergeevich Bykov. On locally balanced gray codes. *Journal of Applied and Industrial Mathematics*, 10(1):78–85, 2016.
- [52] Mari Kobayashi, Giuseppe Caire, and Gerhard Kramer. Joint state sensing and communication: Optimal tradeoff for a memoryless case. In *2018 IEEE International Symposium on Information Theory (ISIT)*, pages 111–115. IEEE, 2018.
- [53] Paolo Valerio Testa, Lazlo Szilagyi, Zoltan Tibensky, Corrado Carta, and Frank Ellinger. A compact vector-sum phase shifter for 5g applications in 22 nm fd-soi cmos. In *2020 IEEE International Symposium on Radio-Frequency Integration Technology (RFIT)*, pages 238–240, 2020.
- [54] Jiangfeng Wu, Acer Chou, Tianwei Li, Rong Wu, Tao Wang, Giuseppe Cusmai, Sha-Ting Lin, Cheng-Hsun Yang, Gregory Unruh, Sunny Raj Dommaraju, Mo M. Zhang, Po Tang Yang, Wei-Ting Lin, Xi Chen, Dongsoo Koh, Qingqi Dou, H. Mohan Geddada, Juo-Jung Hung, Massimo Brandolini, Young Shin, Hung-Sen Huang, Chun-Ying Chen, and Ardie Venes. 27.6 a 4gs/s 13b pipelined adc with capacitor and amplifier sharing in 16nm cmos. In *2016 IEEE International Solid-State Circuits Conference (ISSCC)*, pages 466–467, 2016.
- [55] Xuyuan Liu, Md Hedayatullah Maktoomi, Mahdi Alesheikh, Payam Heydari, and Hamidreza Aghasi. A 49-63 ghz phase-locked fmcw radar transceiver for high resolution applications. In *ESSCIRC 2023- IEEE 49th European Solid State Circuits Conference (ESSCIRC)*, pages 509–512, 2023.

- [56] E. G. Ioannidis, S. Haendler, A. Bajolet, T. Pahron, N. Planes, F. Arnaud, R.A. Bianchi, M. Haond, D. Golanski, J. Rosa, C. Fenouillet-Beranger, P. Perreau, C.A. Dimitriadis, and G. Ghibaud. Low frequency noise variability in high-k/metal gate stack 28nm bulk and fd-soi cmos transistors. In *2011 International Electron Devices Meeting*, pages 18.6.1–18.6.4, 2011.
- [57] Suraj Sindia, Virendra Singh, and Vishwani D Agrawal. Polynomial coefficient based dc testing of non-linear analog circuits. In *Proceedings of the 19th ACM Great Lakes symposium on VLSI*, pages 69–74, 2009.
- [58] Hamidreza Aghasi, Andreia Cathelin, and Ehsan Afshari. A 0.92-thz sige power radiator based on a nonlinear theory for harmonic generation. *IEEE Journal of Solid-State Circuits*, 52(2):406–422, 2017.
- [59] Behnam Moradi, Xuyang Liu, and Hamidreza Aghasi. A 76–82 ghz vco in 65 nm cmos with 189.3 dbc/hz pn fom and -0.6 dbm harmonic power for mm-wave fmcw applications. *IEEE Transactions on Circuits and Systems I: Regular Papers*, 71(1):51–61, 2024.
- [60] Jafar Savoj, Kenny Hsieh, Parag Upadhyaya, Fu-Tai An, Jay Im, Xuewen Jiang, Jalil Kamali, Kang Wei Lai, Daniel Wu, Elad Alon, and Ken Chang. Design of high-speed wireline transceivers for backplane communications in 28nm cmos. In *Proceedings of the IEEE 2012 Custom Integrated Circuits Conference*, pages 1–4, 2012.
- [61] Shubin Liu, Zhangming Zhu, Jingyu Wang, Lianxi Liu, and Yintang Yang. A 1.2-v 2.41-ghz three-stage cmos ota with efficient frequency compensation technique. *IEEE Transactions on Circuits and Systems I: Regular Papers*, 66(1):20–30, 2019.
- [62] Behzad Razavi and Razavi Behzad. *RF microelectronics*, volume 2. Prentice hall New York, 2012.
- [63] Behzad Razavi. Lower bounds on power consumption of clock generators for adcs. In *2020 IEEE International Symposium on Circuits and Systems (ISCAS)*, pages 1–5, 2020.
- [64] Jaspreet Singh, Onkar Dabeer, and Upamanyu Madhow. On the limits of communication with low-precision analog-to-digital conversion at the receiver. *IEEE Trans. on Communications*, 57(12):3629–3639, 2009.
- [65] Hans S. Witsenhausen. Some aspects of convexity useful in information theory. *IEEE Transactions on Information Theory*, 26(3):265–271, 1980.